REMARKS

The Applicants respectfully request reconsideration of the present application in view of the reasons that follow.

I. Status of the claims

No claims are amended, added or canceled in this paper. Accordingly, claims 1-4, 6-7, 11, 14-20, 23, 26-32, 34, 36, 44-55, and 142-144 remain pending in this application, with claims 3, 4, 6, 7 and 142-144 under examination.

II. Claim rejection – 35 U.S.C. § 101

Claims 3, 4, 6, 7 and 142-144 are rejected under 35 U.S.C. § 101 as allegedly failing to meet the utility requirement. Specifically, the Office Action asserts that a skilled artisan would not reasonably conclude that the claimed polynucleotides can be used as a marker for brain tissue because "SEQ ID NO: 56 has a mere 2-fold higher expression in brain than in the reference sample." Office Action at page 3. The Applicants respectfully traverse this ground for rejection.

As noted in the previous reply, credibility is determined by one of ordinary skill in the art. A two-fold difference in expression level is more than sufficient to provide the skilled artisan with a reasonable expectation of successfully distinguishing brain tissue from other tissue types using SEQ ID NO: 56 in a microarray analysis.

Regarding the use of SEQ ID NO: 56 as a marker for brain tissue, the specification describes the microarray analysis which illustrates the tissue-specific expression of SEQ ID NO: 56 as follows.

> RNA samples isolated from a variety of normal human tissues were compared to a common reference sample. Tissues contributing to the reference sample were selected for the ability to provide a complete distribution of RNA in the human body and include brain (4%), heart (7%), kidney (3%), lung (8%), placenta (46%), small intestine (9%), spleen (3%), stomach (6%), testis (9%), and uterus (5%). The normal tissues assayed were obtained from at least three different donors. RNA from each donor was separately isolated and individually hybridized to the microarray. Since these hybridization experiments were conducted using common reference sample, differential expression values are directly comparable from one tissue to another.

Specification at page 102, lines 3-12. Thus, a variety of tissue from "*at least three different donors*" was tested and the expression of SEQ ID NO: 56 was found to be increased by "***at least two-fold***" in brain as compared to the reference sample, which was selected to provide "*a complete distribution of RNA in the human body.*" Specification at page 102, lines 9, 17 and 5-7, respectively.

The Examiner alleges that a "*mere* two-fold increase" in expression level is an insufficient difference to allow the skilled artisan to distinguish brain tissue from other tissues of the body (*e.g.*, heart, kidney, lung, placenta, small intestine, spleen, stomach, testis and uterus). The Applicants respectfully disagree with this blanket characterization of significance and argue that the skilled artisan would consider – and indeed *does* consider – an "*at least two-fold*" difference in expression level significant.

For example, numerous microarray studies have deemed fold-difference values of between 1.4 and 2 fold as significant. *See e.g.*, (1) Yue et al., *Nucleic Acid Research, 29*(8) e41 (2001), reporting a **1.4 fold** change in expression as significant, *see* abstract (EXHIBIT A); (2) Lee et al., *Science, 285*:1390-93, page 1392 (1999), reporting **1.8 fold** induction and **1.6 fold** reduction in gene expression as significant (EXHIBIT B); and (3) Vasseur et al., *Molecular Cancer, 2*(19) (2003), stating at page 2 that "differential expression values of greater than **1.7** are likely to be significant, based on internal quality control data," however, that a "more stringent

ratio" of "at least 2.0 fold" was used (EXHIBIT C). Indeed, reviews on the topic conclude that "there is no magical absolute cut-off for a meaningful fold value" and that essentially, the parameters of each analysis must be considered in determining a meaningful cut-off value for that particular analysis. *See e.g.*, Tsien et al., "On reporting fold differences," *Pacific Symposium on Biocomputing*, *6*:496-507, at 504 (2001), (EXHIBIT D). Accordingly, the skilled artisan would consider an expression differential of "at least two-fold" a more than reasonable cut-off to distinguish brain tissue from other tissue types in a microarray analysis using SEQ ID NO: 56. As such, the noted utility is **credible**.

The Applicants respectfully contend that the Examiner impermissibly raises the utility standard to something which it is not. With respect to utility, the M.P.E.P. states as follows:

> The claimed invention must only be capable of performing *some beneficial function*...An invention does not lack utility merely because the particular embodiment disclosed in the patent *lacks perfection or performs crudely*....*A commercially successful product is not required*....Nor is it essential that the invention accomplish all its intended functions...or operate under all conditions ...*partial success being sufficient to demonstrate patentable utility*...In short, the defense of non-utility cannot be sustained *without proof of total incapacity*. *If an invention is only partially successful in achieving a useful result, a rejection of the claimed invention as a whole based on a lack of utility is not appropriate.*

M.P.E.P. § 2107.01.II (citations omitted, emphasis added). Thus, while a higher "fold difference" may be required in some circumstances - *e.g.*, FDA approval - such conditions are not required to meet the utility requirement under 35 U.S.C. § 101. In the present case, the expression level of SEQ ID NO: 56 is "at least two-fold higher" in brain tissue as compared to the control sample, and the art supports the "at least two-fold" difference in expression to be significant, *i.e.*, credible.

Accordingly, for at least the reasons stated above, the claimed invention has a specific, substantial and credible utility, and reconsideration and withdrawal of the rejection under 35 U.S.C. § 101 is respectfully requested.

III. Claim rejection – 35 U.S.C. § 112, first paragraph

Claims 3, 4, 6, 7 and 142-144 are rejected under 35 U.S.C. § 112, first paragraph, as allegedly failing to meet the enablement requirement. The Office Action asserts that "since the claimed invention is not supported by either a specific and substantial asserted utility or a well-established utility...one skilled in the art would not know how to use the claimed invention." Office Action at page 3. The Applicants respectfully traverse this ground for rejection.

As noted above in section II, the claimed invention has a specific, substantial and credible utility. Accordingly, the reason for rejection is moot, and reconsideration and withdrawal is respectfully requested.

IV. Conclusion

The present application is now in condition for allowance. Favorable reconsideration of the application is respectfully requested.

The Examiner is invited to contact the undersigned by telephone if it is felt that a telephone interview would advance the prosecution of the present application.

The Commissioner is hereby authorized to charge any additional fees which may be required regarding this application under 37 C.F.R. §§ 1.16-1.17, or credit any overpayment, to Deposit Account No. 19-0741. Should no proper payment be enclosed herewith, as by the credit card payment instructions in EFS-Web being incorrect or absent, resulting in a rejected or incorrect credit card transaction, the Commissioner is authorized to charge the unpaid amount to Deposit Account No. 19-0741.

If any extensions of time are needed for timely acceptance of papers submitted herewith, the Applicants hereby petition for such extension under 37 C.F.R. § 1.136 and authorize payment of any such extensions fees to Deposit Account No. 19-0741.

Respectfully submitted,

Date: January 13, 2010

By: /Stephanie H. Vavra/ Reg. No. 45,178

FOLEY & LARDNER LLP
Customer Number: 22428
Telephone: (202) 672-5538
Facsimile: (202) 672-5399

for Michele M. Simkin
Attorney for the Applicants
Registration No. 34,717

Nucleic Acids Research, 2001, Vol. 29, No. 8 e41

An evaluation of the performance of cDNA microarrays for detecting changes in global mRNA expression

Huibin Yue, P. Scott Eastman*, Bruce B. Wang, James Minor, Michael H. Doctolero, Rachel L. Nuttall, Robert Stack, John W. Becker, Julie R. Montgomery, Marina Vainer and Rick Johnston

Advanced Research Group, Incyte Genomics, 6519 Dumbarton Circle, Fremont, CA 94555, USA

Received as resubmission February 13, 2001; Accepted February 18, 2001

ABSTRACT

The cDNA microarray is one technological approach that has the potential to accurately measure changes in global mRNA expression levels. We report an assessment of an optimized cDNA microarray platform to generate accurate, precise and reliable data consistent with the objective of using microarrays as an acquisition platform to populate gene expression databases. The study design consisted of two independent evaluations with 70 arrays from two different manufactured lots and used three human tissue sources as samples: placenta, brain and heart. Overall signal response was linear over three orders of magnitude and the sensitivity for any element was estimated to be 2 pg mRNA. The calculated coefficient of variation for differential expression for all non-differentiated elements was 12–14% across the entire signal range and did not vary with array batch or tissue source. The minimum detectable fold change for differential expression was 1.4. Accuracy, in terms of bias (observed minus expected differential expression ratio), was less than 1 part in 10 000 for all non-differentiated elements. The results presented in this report demonstrate the reproducible performance of the cDNA microarray technology platform and the methods provide a useful framework for evaluating other technologies that monitor changes in global mRNA expression.

INTRODUCTION

The construction of gene expression databases is a high priority of today's research community. Such databases, closely integrated with other types of genomic information, promise not only to facilitate our understanding of many fundamental biological processes, but also to accelerate drug discovery and lead to customized diagnosis and treatment of disease (1–6).

These databases will require the development of one or more underlying supporting technologies that can accurately and reproducibly measure changes in global mRNA expression levels. The ideal technology should be able to process large numbers of samples, require minimal amounts of biological source material and be applicable across a wide range of cell or tissue types. Several different technologies are currently being investigated for their ability to meet these stringent requirements (7–12). While many of these technologies show significant promise in preliminary studies, it is critically important that each technology be comprehensively evaluated as a complete system for producing accurate, precise and reliable expression data (13,14).

The Incyte cDNA microarray technology platform simultaneously analyzes the relative expression levels of up to 10 000 genes, each of which is present as a unique cDNA element (7). The platform is potentially scalable to include all of the elements in the human genome. PCR-derived elements averaging 1000 nt in length are physically arrayed in a two-dimensional grid on a chemically modified glass slide. Aliquots from two purified mRNA samples are separately reverse transcribed using primer sets labeled with two different fluorophores and the resulting dye-labeled cDNA populations are used to probe the target elements in a competitive hybridization reaction. After hybridization the glass slide is analyzed in a two-channel fluorescence scanner and the ratio between the two fluorophores detected for any given element defines the relative amount of the mRNA corresponding to that element present in the original two samples.

There are many process variables that will impact on the quality of the data generated by any microarray technology platform. In this report we describe parameters for the manufacture of effective cDNA microarrays with highly reproducible performance characteristics, the quality and quantity of sample mRNAs used to create the dye-labeled cDNA probe and the effects of these optimized procedures on the overall performance, accuracy, precision and reliability of expression data generated from the two-channel ratiometric approach.

MATERIALS AND METHODS

Synthesis of PCR products

PCR was used to generate large quantities of defined target DNA for microarray production. Plasmids containing cloned genes were grown in *Escherichia coli* and were amplified using vector primers SK536 (5′-GCGAAAGGGGGATGT-GCTG-3′) and SK865 (5′-GCTCGTATGTTGTGTGGAA-3′)

*To whom correspondence should be addressed. Tel: +1 510 739 2172; Fax: +1 510 739 2250; Email: seastman@incyte.com

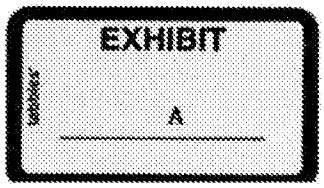

(Operon Technologies, Alameda, CA). Briefly, 1 µl of bacterial cell culture was added to 75 µl of reaction buffer, containing 10 mM Tris–HCl pH 8.3, 1.5 mM $MgCl_2$, 50 mM KCl, 0.2 mM each dNTP, 0.5 µM each primer and 2 U *Taq* polymerase. The mixture was incubated for 3 min at 95°C and 30 cycles of PCR were performed at 94°C for 30 s, 56°C for 30 s and 72°C for 90 s. A final incubation for 5 min at 72°C was followed by reduction of the temperature to 4°C in order to terminate the reaction. PCR products were then purified by centrifugal chromatography with Sephadex S400 resin (Amersham-Pharmacia Biotech, Uppsala, Sweden) in a 96-well format. Briefly, 400 µl of S400 resin pre-equilibrated in 0.2× standard saline citrate buffer (SSC) was added to each well of a 96-well microtiter plate. A unique PCR product prepared as described above was loaded into each well and the plate was centrifuged in an Eppendorf 5810 centrifuge at 885 r.c.f. (relative centrifugal force). Purified PCR products were concentrated to dryness and resuspended in 10 µl of H_2O. DNA was resolubilized by thermal cycling (five cycles of 85°C for 30 s and 20°C for 30 s).

Qualification and quantification of PCR products

PCR products were routinely analyzed for quality by agarose gel electrophoresis and samples that failed to amplify or had multiple bands were annotated in the GEMTools database management software (Incyte Genomics, Fremont, CA). PCR products were quantified using PicoGreen dye (Molecular Probes, Eugene, OR) in a fluorescent assay specific for measuring double-stranded DNA concentration according to the manufacturer's instructions.

Arraying and post-processing

Ten thousand PCR products were arrayed by high speed robotics (7) on amino-modified glass slides (M.Reynolds, unpublished results). Each element occupied a spot of ~150 µm in diameter and spot centers were 170 µm apart. DNA adhesion to the glass was achieved by irradiation in a Stratalinker Model 2400 UV illuminator (Stratagene, San Diego, CA) with light at 254 nm and an energy output of 120 000 µJ/cm^2. To minimize any potential non-specific probe interactions with the glass the microarrays were washed for 2 min in 0.2% SDS (Life Technologies, Rockville, MD), followed by three rinses in H_2O for 1 min each. The microarrays were treated with 0.2% (w/v) I-block (Tropix, Bedford, MA) in phosphate-buffered saline (PBS) for 30 min at 60°C. They were washed again for 2 min in 0.2% SDS, rinsed three times in H_2O for 1 min each and finally dried by a brief centrifugation. Dried microarrays were routinely stored in opaque plastic slide boxes at room temperature.

Array qualification: SYTO 61 dye

As SYTO 61 nucleic acid staining has generally been applied to cells, the standard procedure was modified to allow its use for measurement of DNA bound to microarrays. A 5 µM stock solution of SYTO 61 dye (Molecular Probes) in DMSO was diluted 1:100 in 10 mM Tris–HCl pH 7, 0.1 mM EDTA (TE). Several microarrays from each manufactured batch were immersed in this solution for 5 min at room temperature, rinsed with TE, rinsed with H_2O and finally with absolute ethanol. After drying the microarrays were scanned on a GenePix 4000A scanner (Axon Instruments, Foster City, CA) at 535 nm.

mRNA preparation and probe synthesis

Briefly, mRNA was isolated by a single round of poly(A) selection using Oligotex resin (Qiagen, Valencia, CA) from commercially available human placenta, brain and heart total RNA (Biochain, San Leandro, CA). The purified mRNA was quantified using RiboGreen dye (Molecular Probes) in a fluorescent assay. RiboGreen dye was diluted 1:200 (v/v final) and mixed with known RNA concentrations (determined by absorbance at 260 nm) ranging from 1 to 5000 ng/ml. A Millennium RNA size ladder (Ambion, Austin, TX) was used to generate standard curves and unknown samples were diluted as necessary. Fluorescence was measured in 96-well plates with a FLUOstar fluorometer (BMG Lab Technologies, Germany) fitted with 485 nm (excitation) and 520 nm (emission) filters.

Between 25 and 100 ng mRNA were separated on an Agilent 2100 Bioanalyzer, a high resolution electrophoresis system (Agilent Technologies, Palo Alto, CA), to examine the mRNA size distribution. 200 ng of purified mRNA were converted to either a Cy3- or Cy5-labeled cDNA probe using a custom labeling kit (Incyte Genomics). Each reaction contained 50 mM Tris–HCl pH 8.3, 75 mM KCl, 15 mM $MgCl_2$, 4 mM DTT, 2 mM dNTPs (0.5 mM each), 2 µg Cy3 or Cy5 random 9mer (Trilink, San Diego, CA), 20 U RNase inhibitor (Ambion), 200 U MMLV RNase H-free reverse transcriptase (Promega, Madison, WI) and mRNA. Correspondingly labeled Cy3 and Cy5 cDNA products were combined and purified on a size exclusion column, concentrated by ethanol precipitation and resuspended in hybridization buffer.

Array qualification: complex and vector-specific hybridizations

Hybridization of labeled cDNA probes was performed in 20 µl of 5× SSC, 0.1% SDS, 1 mM DTT at 60°C for 6 h. Hybridization with a Cy3-labeled vector-specific oligonucleotide (5′-TTCG-AGCTTGGCGTAATCATGGTCATAGCTGTTTCCTGTGT-GAAATTGTTATCCGCTCA-3′) (Operon Technologies) was performed at 10 ng/µl in 5× SSC, 0.1% SDS, 1 mM DTT at 60°C for 1 h. The microarrays were washed after hybridization in 1× SSC, 0.1% SDS, 1 mM DTT at 45°C for 10 min and then in 0.1× SSC, 0.2% SDS, 1 mM DTT at room temperature for 3 min. After drying by centrifugation, microarrays were scanned with an Axon GenePix 4000A fluorescence reader and GenePix image acquisition software (Axon) at 535 nm for Cy3 and 625 nm for Cy5. An image analysis algorithm in GEMTools software (Incyte Genomics) was used to quantify signal and background intensity for each target element. The ratio of the two corrected signal intensities was calculated and used as the differential expression ratio (DE) for this specific gene in the two mRNA samples.

The Axon scanner was calibrated using a primary standard and a secondary standard to account for the differences in scanner performance [laser and photomultiplier tube (PMT)] between the Cy3 and Cy5 channels. For the primary standard hundreds of probe samples were prepared that were fluorescently balanced in the Cy3 and Cy5 channels as determined by a Fluorolog3 fluorescence spectrophotometer (Instruments SA, Edison, NJ). These probes were hybridized to microarrays and the scanner PMTs were adjusted to give balanced fluorescence and the greatest dynamic range. Using these PMT values

a fluorescent plastic slide was scanned to obtain corresponding fluorescent values. This secondary standard was used to calibrate scanners on a daily basis.

Data acquisition and analysis

Two low frequency data correction algorithms were applied to compensate for systematic variations in data quality. The first procedure, a gradient correction algorithm, modeled the signal response surfaces of each channel. On a 10 000 element microarray the signal responses of Cy3 and Cy5 should be random due to the random physical location of the target elements. The signal response surfaces were first examined for non-random patterns. If non-random patterns were detected, a second order response model was applied to model the gene signal responses according to their positions on the surface. The non-randomness was then corrected using the fitted model. The second procedure, a signal correction algorithm, corrected for differential rates of incorporation of the Cy3 and Cy5 dyes. In an idealized homotypic hybridization, a scatter plot of log Cy3 signal versus log Cy5 signal should show a signal distribution along a line with a slope of 1. If the center line of the signals does not have a slope of 1 there may be different rates of incorporation of the Cy3 and Cy5 dyes. The signal correction algorithm tested whether the slope of the regression line for log Cy3 signal versus log Cy5 signal was 1 and applied a regression model to rotate the regression line to a slope of 1 if necessary.

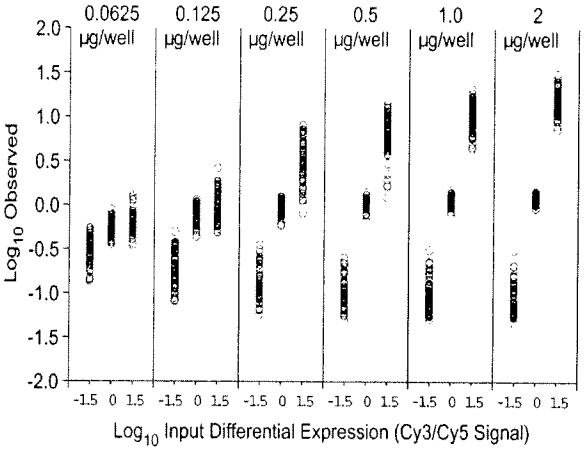

Figure 1. Impact of input DNA concentration on differential gene expression. A dilution series of PCR product for three yeast control fragments was arrayed in triplicate in each of four quadrants. The amount of PCR product in the well prior to arraying is indicated above each panel. Input RNA ratios for labeling with Cy3 versus Cy5 for the three fragments were 30:1, 1:1 and 1:30. The $\log_{10}$ of observed differential expression is plotted as a function of $\log_{10}$ of input RNA ratios.

RESULTS AND DISCUSSION

Impact of arrayed DNA concentration on DEs

Because of the competitive nature of two channel fluorescent hybridizations it has been assumed that the amount of target DNA deposited on the glass slide would have little or no impact on any observed DEs (15). We tested this assumption directly by hybridizing a series of samples at predetermined input ratios to microarrays containing varying amounts of target DNA. For these experiments the target DNAs were yeast fragments, a set of PCR products derived from the non-coding regions of *Saccharomyces cerevisiae*. The amount of PCR product was quantified using a fluorescent dye (PicoGreen) specific for double-stranded DNA. The targets were spotted in three sets containing quadruplicate points from a 2-fold dilution series of DNA concentrations ranging from 2.0 to 0.062 µg/well (10 µl/well).

Probes for hybridization to the yeast fragments were made from T7 RNA transcripts of PCR products. Templates for *in vitro* transcription were made by incorporating a T7 promoter in the upstream PCR primer and poly(A) sequences in the downstream PCR primer. *In vitro* transcripts of the yeast fragments were purified, quantified and included in every labeling reaction at predetermined Cy3:Cy5 input levels (fragment 22, 123:4 pg; fragment 6, 123:123 pg; fragment 25, 4:123 pg). All probe labeling reactions were done in the presence of 200 ng poly(A) mRNA, from either human brain or heart (Biochain, Hayward, CA). Hybridization of these probes was performed on three different days, across 20 microarrays representing two different batches and by multiple operators. A comparison of the expected differential expression and the experimentally observed differential expression is shown in Figure 1. These results indicate that target DNA arrayed at input concentrations <1.0 µg/10 µl results in an underestimate or compression of the observed differential expression, with more compression occurring at lower DNA concentrations.

Quantification of DNA amplimers on the array by a hybridization-independent method

The DNA concentration of the input printing solutions may not be directly predictive of the amount of DNA actually retained on the glass. Variations in the transfer efficiency of individual DNA sequences to the glass and variations in its subsequent retention through the post-arraying and processing procedures may have an impact on the amount of DNA retained. Therefore, a second DNA staining assay was developed using SYTO 61 fluorescent dye, which directly measured the amount of DNA actually retained on the glass, independent of hybridization.

Qualification of 10 000 element cDNA microarrays

Based on the preliminary experiments we applied the PicoGreen and SYTO 61 assays to evaluate two independent 10 000 element microarrays (Fig. 2). Each of the 104 96-well plates used to print the arrays was qualified by PicoGreen analysis and all plate sets had high levels of PCR amplimer (>1.0 µg/well) (Fig. 2A). The plate sets used to prepare the HGG1 arrays, however, had a greater overall average DNA concentration than those used to prepare the UGV1 arrays: median 3.6 versus 1.85 µg/well, respectively.

An array from each batch was hybridized with a complex cDNA probe derived from placenta RNA in both the Cy3 and Cy5 channels. SYTO 61 staining was performed on an additional array from each batch and a comparison of the signal outputs for SYTO 61 and hybridization probes for both array batches is shown in Figure 2B and C. Observed hybridization signals were generally higher for the HGG1 array (Fig. 2C) as

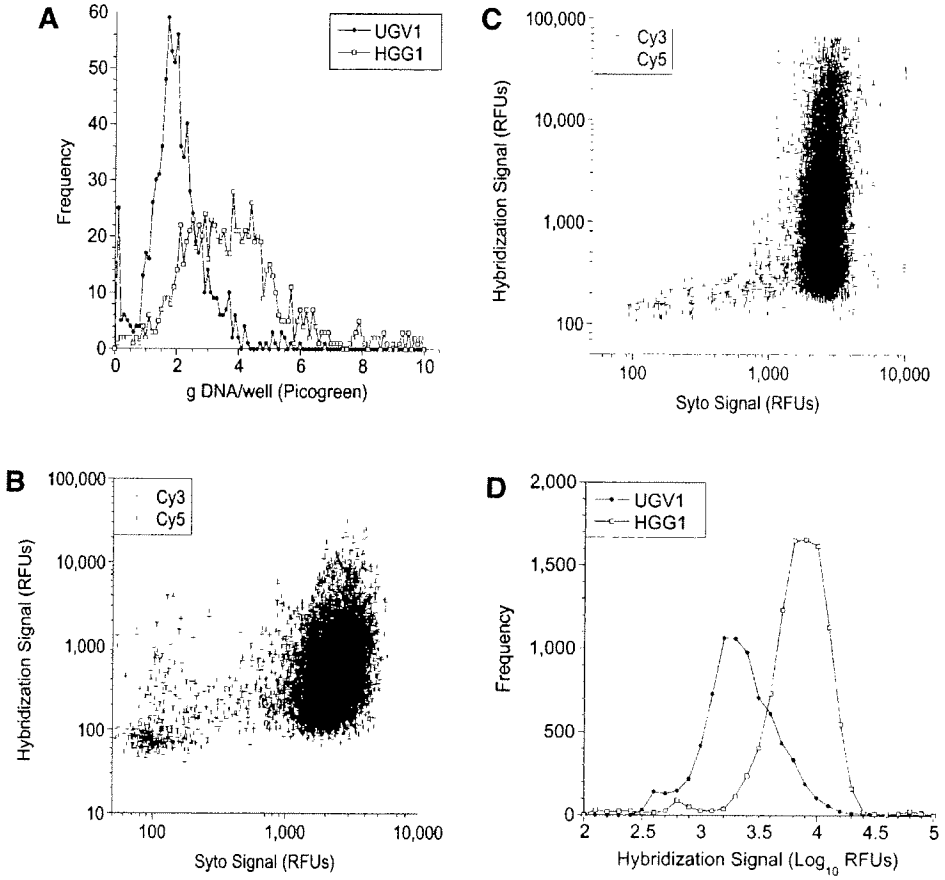

Figure 2. Quality control analysis of microarray batches. A set of eight wells randomly selected from each of 104 96-well plates from microarray types UGV1 and HGG1 was analyzed with PicoGreen. The distribution of DNA concentrations is shown in (**A**). The amount of hybridization signal with a complex probe (Cy3 Brain/Cy5 Heart) is shown as a function of the amount of DNA retained on the glass for microarray types UGV1 (**B**) and HGG1 (**C**). Signal distributions from hybridizations with a vector-specific oligonucleotide probe for each array type are shown in (**D**).

compared to the UGV1 array (Fig. 2B): median Cy3 1049 versus 310 relative fluorescence units (r.f.u.), median Cy5 1137 versus 302 r.f.u., respectively. This was consistent with the higher amount of DNA on the glass for the HGG1 array: median 2532 versus 1905 r.f.u. Higher hybridization signals (>10 000 r.f.u.) were routinely observed when the amount of target DNA bound to the glass approached 2000 r.f.u. by SYTO 61 staining (data not shown). In the examples shown, 35% of the elements on the UGV1 microarray have SYTO 61 stain values <2000 r.f.u., as compared to only 9% of the elements on the HGG1 array. There was an apparent discrepancy in the UGV1 microarray, 65% of all elements on the UGV1 array having higher levels of bound DNA but few yielding hybridization signals >10 000 r.f.u..

To address this issue a third assay was developed. An array from each batch was hybridized with a Cy3-labeled oligonucleotide probe specific for the common vector sequence found in all the PCR products. The signal distribution for these vector hybridizations is presented in Figure 2D. The majority of elements on the UGV1 microarray had significantly lower hybridization signals than the HGG1 array: median 1901 versus 6507 r.f.u. These results correlated better with complex probe hybridization than SYTO 61 staining (Fig. 2B and C).

The manufacture of high quality, reproducible arrays with 10 000 or more unique PCR products is an expensive and time-consuming effort. It requires considerable attention to the details of each step in the process and defined procedures to ensure quality and reproducibility. The data presented in this report show that low concentrations of DNA in the input printing solutions result in reduced amounts of arrayed DNA and this, in turn, reduces the dynamic signal range and produces an apparent compression or underestimation of differential expression. The assay procedures reported here have been implemented in the large-scale production of microarrays for use in generating expression databases.

mRNA input

The impact of varying the amount of input mRNA on net cDNA probe synthesis and hybridization was evaluated. Placental mRNAs of varying amounts (25–400 ng) were

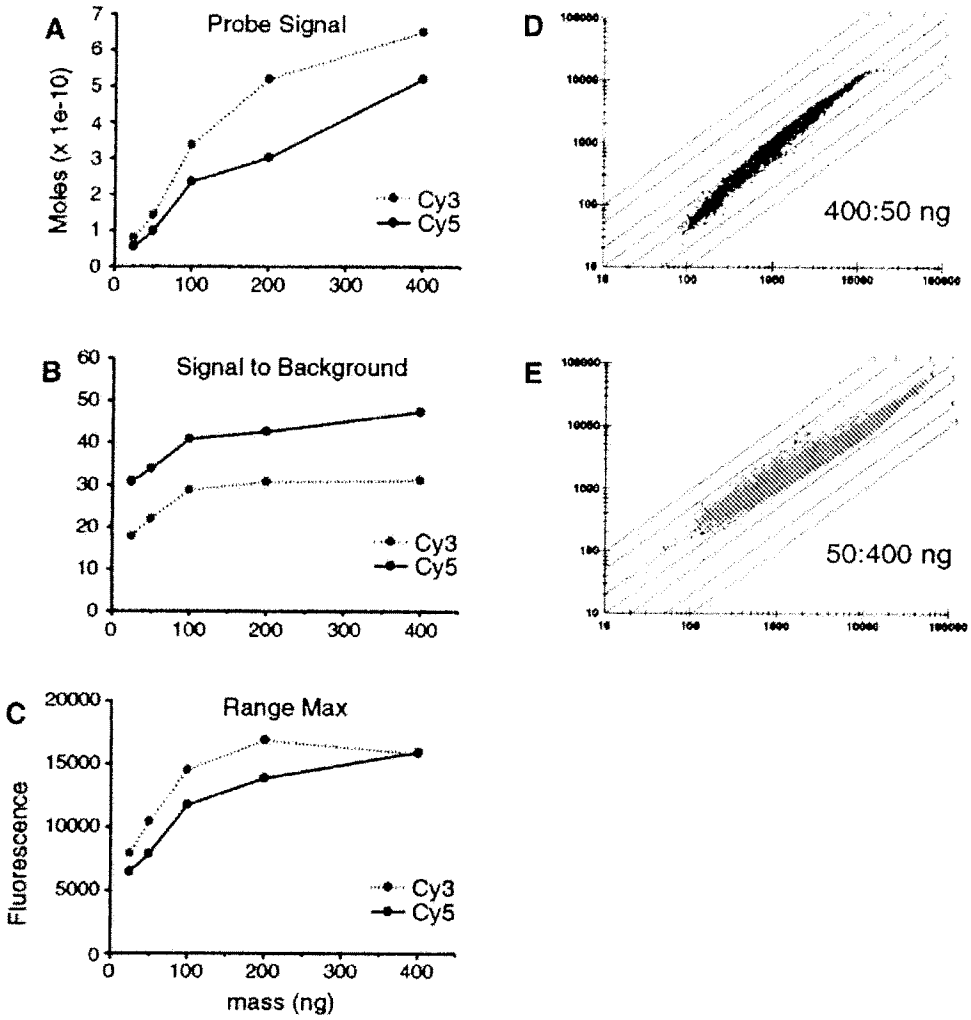

Figure 3. mRNA titration and balance. (**A–C**) Probe fluorescent signals, signal-to-background and dynamic range as a function of input mRNA mass. Duplicate labeling reactions containing equal amounts of placenta mRNA in both the Cy3 and Cy5 channels were labeled and hybridized to UniGEM V2 arrays. Each data point is an average from the two hybridizations. Probe fluorescence signal was converted to moles product using a standard curve. Range minimum values remained between 100 and 200 U for all hybridizations. (**D** and **E**) An aliquot of 50 or 400 ng placenta mRNA was labeled with Cy3 and hybridized to either 400 or 50 ng mRNA labeled with Cy5, respectively, in duplicate. Only one of the two hybridizations is shown. The axes are in arbitrary fluorescent units.

labeled with Cy3 and hybridized to an equal aliquot labeled with Cy5. Increasing the placental mRNA input yielded increasing amounts of total cDNA product (Fig. 3A). Hybridization signal-to-background and dynamic range also increased as the mRNA input increased, although a clear point of 'diminishing returns' occurs above 200 ng mRNA input (Fig. 3B and C). Based on this mRNA titration series, we believe that using 200 ng mRNA as the standard input for labeling reactions is the optimal amount. A representative example of a competitive hybridization with balanced RNA inputs (200:200 ng) is presented in Figure 4A.

We tested the effect of unbalanced competitive hybridization by hybridizing product prepared from different input levels of placental mRNA in the labeling process (Fig. 3D and E). We observed significant loss in precision and a distortion of the population from the theoretical DE of 1, especially in the lower signal range. This distortion reflects both the impact of differential labeling and hybridization of transcripts with different amounts of mRNA input. Reversing the ratio of input mRNA for probe synthesis resulted in the opposite curvature (Fig. 3E). We conclude that accurate quantification and use of an equivalent mRNA mass for labeling in both channels is essential for optimum results.

Homotypic response

An estimate of the accuracy and precision of array-generated expression data was first made by performing a series of replicate experiments using various homotypic hybridizations. A competitive hybridization of fluorescently labeled Cy3 and Cy5 cDNA, both prepared from the same placental mRNA,

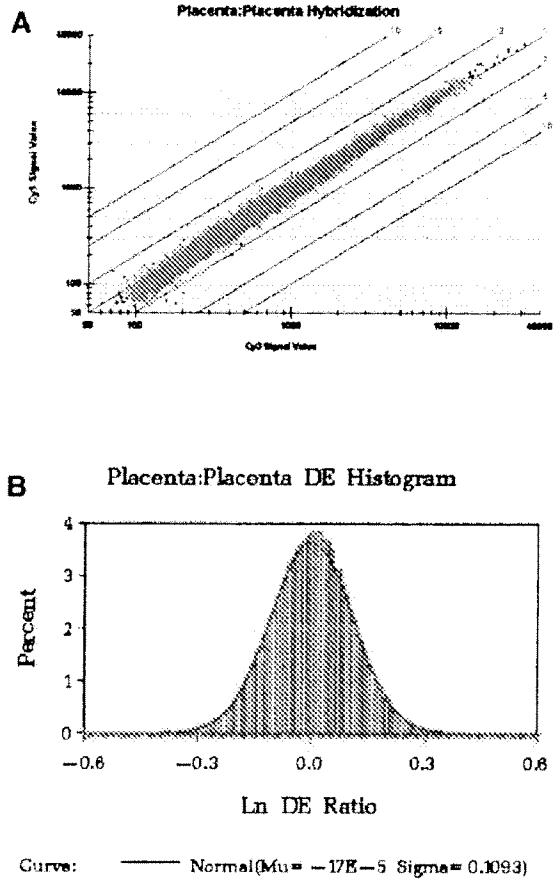

Figure 4. (**A**) Scatter plot of the calibrated Cy3 versus Cy5 fluorescence response from a typical placenta:placenta hybridization. The diagonal line through the origin corresponds to the expected DE of 1. The other diagonal lines define DE values as indicated next to the line. (**B**) Histogram showing the distribution of elements by $\log_n$ of their experimentally derived DEs for 10 homotypic placental hybridizations.

should theoretically give a DE (or Cy3 fluorescence divided by Cy5 fluorescence) of 1 for all 10 000 elements arrayed on the slide. With replicate hybridizations we can evaluate the overall precision of the data using various statistical parameters and obtain an estimate of accuracy from any deviation(s) observed from the theoretical value.

A scatter plot of the Cy3- versus Cy5-calibrated fluorescent response from a single placenta:placenta hybridization is shown in Figure 4A. Virtually all gene elements lie close to the diagonal line corresponding to the expected DE of 1. Overall system response was observed to be linear over about three orders of magnitude.

Approximately 100 000 data points from 10 homotypic placenta hybridizations were used to construct a histogram showing the frequency or distribution of gene elements (as a percentage of the total) around $\log_n$ of the expected DE (ln 1.0 = 0). Effectively, the histogram (Fig. 4B) is a graphical measure of the range of the signal response for each selected element. The coefficient of variation (CV), or relative standard deviation, provides a quantitative estimate of the precision of differential expression. The calculated CV for differential expression for all elements was 12% across the entire signal range. The same 12% variance was observed across two independently manufactured batches of cDNA microarrays (data not shown).

Ten similar homotypic hybridization experiments were conducted with both human brain and heart samples and the data were compared to the placenta results described above. Results for both sets of hybridizations were identical (data not shown). The same 12% CV for differential expression was observed independent of tissue type over the entire signal range.

Accuracy, in terms of bias, was estimated by calculating an average experimental DE directly from observed fluorescence output and comparing it to the expected value of 1.00. For each of the three tissue types above (placenta, brain and heart) the average (n = 10) experimental DE values were 0.999983, 0.99977 and 0.9998, respectively. The overall average was 0.9999, or less than 1 part in 10 000. These values are in good agreement not only within the group, but also with the expected theoretical value of 1.00.

The observed variation in individual element responses (from the expected DE = 0) for 180 randomly selected genes across the full range of observed signal response (as a function of Cy5 signal) is shown in Figure 5A–C for placenta, brain and heart tissue. For each of the 180 elements selected all 10 replicate data points are plotted for each gene from each tissue type. Regardless of tissue type we observed few data points with a differential expression greater than 2, even at low overall signal levels.

From the above data we can calculate the change in DE required before the value has statistical significance. Mathematically this can be written in terms of the two-sided statistical tolerance interval for the differential expression of non-differentiated elements (16). A statistical tolerance interval is one that contains a specified portion, p, of the entire sampled population with a specified degree of confidence, $100(1-q)\%$. Table 1 shows the 99.5% tolerance intervals for 99% of the elements from each tissue type: all observed differential expression values fall between ±1.4.

Analysis of variance (ANOVA) was used to estimate the contribution of specific potential sources of variance to the overall variance measured. Analyses were performed using the method of restricted maximum likelihood under SAS for Windows v.6.12 procedure PROC MIXED (17). All of the homotypic placenta, brain and heart data sets were used for this analysis.

There are four general sources of variation in the DE ratios: microarray batch, array-to-array hybridization variance (including sample preparation), biological source tissue and gene sequence variance. Table 2 lists the estimated contribution of these potential sources of variation to the overall variance measured. The two sources contributing most significantly to the overall variation were hybridization variance and sequence variance. Hybridization variance represents a source of variation from hybridization to hybridization. Sequence variance indicates that different elements demonstrate different levels of variation. Microarray batches and source tissues were not significant sources of variance.

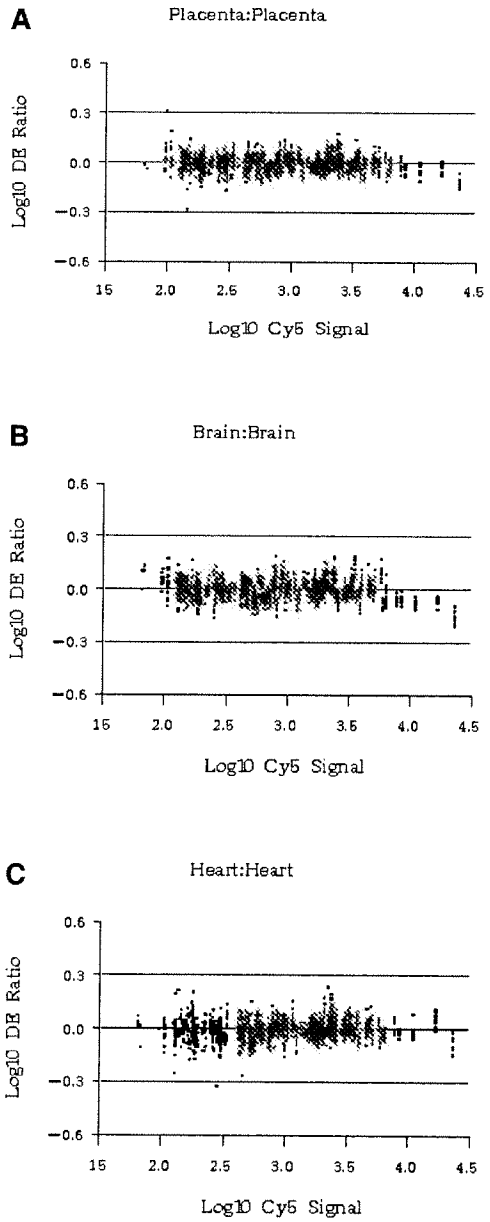

Figure 5. Variation in individual element responses for 180 randomly selected genes over the full range of observed signal response (expressed as log Cy5 signal). All 10 replicate data points for each selected element are plotted along the vertical axis. Horizontal lines define the tolerance interval outside of which DE was deemed significant (see text). (**A**) Homotypic placental hybridizations. (**B**) Homotypic brain hybridizations. (**C**) Homotypic heart hybridizations.

Differential expression

Using placental mRNA as a common reference, four sets of experimental conditions to measure differential expression were evaluated. Each set contained 10 replicate hybridizations: brain:placenta, placenta:brain, heart:placenta and placenta:heart. Estimates of system precision and detection limits were made as described above for the homotypic hybridizations.

Table 1. Tolerance intervals for homotypic hybridizations

Source	Tolerance interval
Placenta:placenta	(−1.332, 1.332)
Brain:brain	(−1.397, 1.397)
Heart:heart	(−1.384, 1.384)
All combined	(−1.370, 1.370)

The 99.5% tolerance intervals contain at least 99% of the elements on each microarray.

Table 2. Variance component estimation for homotypic hybridizations

Variation source	Estimated CV contribution
Microarray batch	0.0%
Source tissue	0.0%
Hybridization	7.8%
Gene sequence	9.4%
Total	12.0%

ANOVA was performed on placenta, brain and heart homotypic hybridizations.

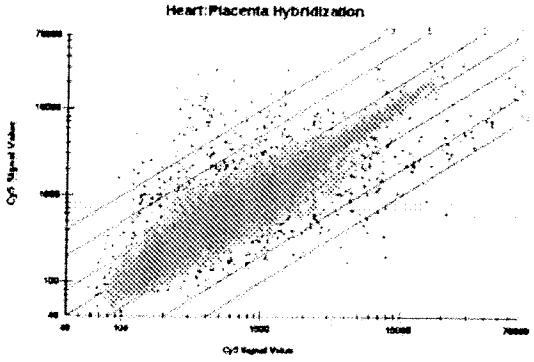

Figure 6. Scatter plot of Cy3-labeled cDNA from heart (*x*-axis) hybridized to the array with Cy5-labeled cDNA from placenta (*y*-axis) (single experiment). Compare with Figure 4A.

Figure 6 shows the fluorescence response plot of a single representative experiment conducted with Cy3-labeled cDNA from heart competitively hybridized to the array with Cy5-labeled cDNA prepared from placenta. Most of the elements (>90%) fell on or close to the 45° line representing no differential expression (or DE = 1.00). However, in contrast to the homotypic hybridizations (Fig. 4A), 10% of the elements were also observed to fall outside the tolerance interval, which may indicate significant differential expression (Table 1).

From 10 such replicate experiments in this set we calculated a CV for each of the 10 000 elements and plotted the values against the overall dynamic signal range (as a function of log Cy5 fluorescence signal) as shown in Figure 7A. The average CV was observed to be 10–12% across the entire signal range, although there was slightly greater variation at low signal

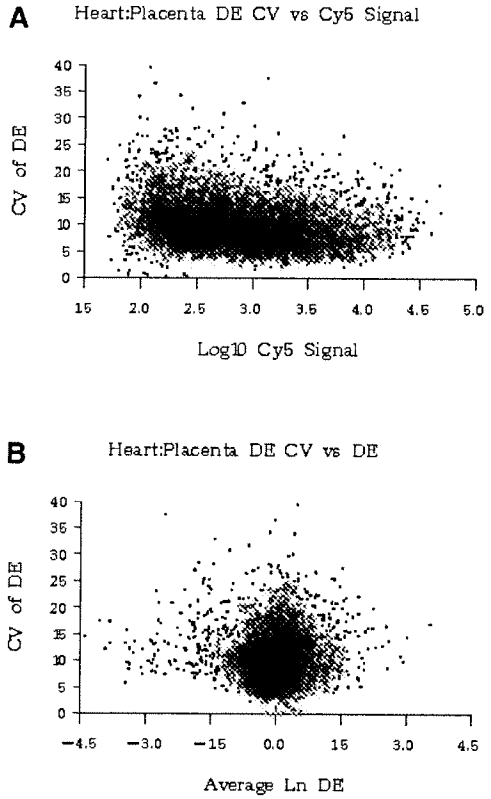

Figure 7. (**A**) CV for each of 10 000 elements derived from 10 replicate heart:placenta hybridizations plotted as a function of the average observed signal (as Cy5 signal). (**B**) CV for the same 10 000 elements plotted as a function of $\log_n$ of the average observed DE (ln DE).

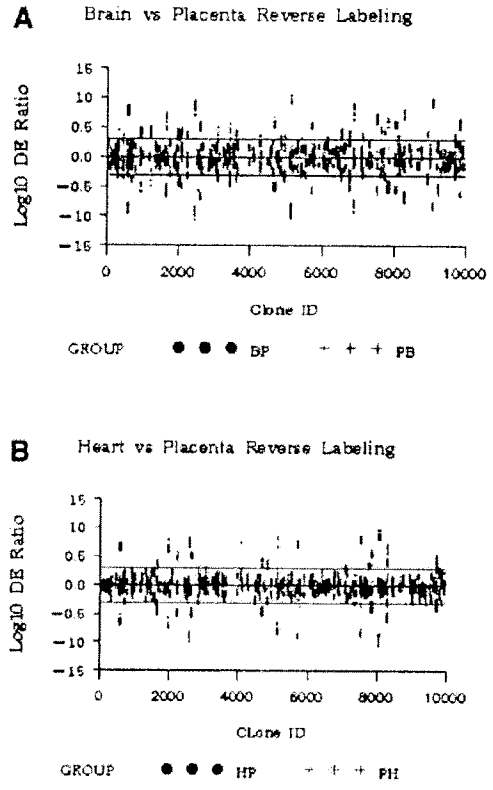

Figure 8. Reciprocal labeling experiments showing the data plotted from 180 random elements from (**A**) 10 replicate brain:placenta (black symbols) and 10 replicate placenta:brain (blue symbols) hybridizations versus log DE, and (**B**) 10 replicate heart:placenta (black) and 10 replicate placenta:heart (blue) hybridizations.

levels. Figure 7B shows the CV for the same 10 000 elements above plotted as a function of average DE. Most elements are observed to cluster near the value 0, indicating no differential expression. However, the CV of 12% observed for non-differentiated elements, on average, was slightly smaller than the CV for differentiated elements in either direction. The observed average CV ranged from 12% for non-differentiated elements to a maximum value of 25% for elements differentially expressed by a factor of 100. Since the DE is a ratio of the signals from the two channels, variations in the denominator at lower signal levels have a larger impact. Despite these minor differences, overall system precision remains excellent.

The same 180 random elements in Figure 5 were evaluated in 'reciprocal dye labeling' experiments. Theoretically, the Cy3- and Cy5-labeled primers should function equivalently for cDNA synthesis. However, any differences in incorporation of label would, if significant, identify differential expression where none exists. It could also account for some of the variation we observe in the different parameters evaluated in this study. Therefore, we performed a series of additional experiments specifically designed to address this issue.

The data from 10 replicates of the brain:placenta hybridizations were compared to the data from 10 replicates of the reciprocally labeled placenta:brain hybridizations. Figure 5A shows a plot of the DE for 180 random elements from both sets of data. The DE for any given element in the first set of hybridizations should simply be the reciprocal of the DE for the same element in the second set (when the labeling is reversed). As Figure 8A shows, the cluster of 10 data points for each element from set 1 lies the same distance above the horizontal line through $\log_{10}$ 1.0 = 0 as the corresponding cluster from set 2 lies below it. Figure 8B shows a similar plot generated from 20 microarrays, where 10 heart:placenta hybridizations were compared to the reciprocally labeled placenta:heart hybridizations, with essentially equivalent results.

For each element we can define the axial symmetry of reflection (ASR) as the inflection point between the DEs from the reciprocal labeling experiments, calculated by averaging the two DE ratios. Calculated average ASR values of 0.998 and 0.999 were obtained from the placenta:brain and placenta:heart data sets, respectively, in good agreement with the theoretical value of 1.00. Thus any systematic bias introduced into the DE by reciprocal labeling must be less than 1–2 parts in 1000. These results independently verify the precision in measuring differential expression, as well as in identifying those genes that are not differentially expressed. Histograms showing the distribution of all elements (as a percentage of the total) as a function of ln ASR (Fig. 9A and B) were similar to the histogram

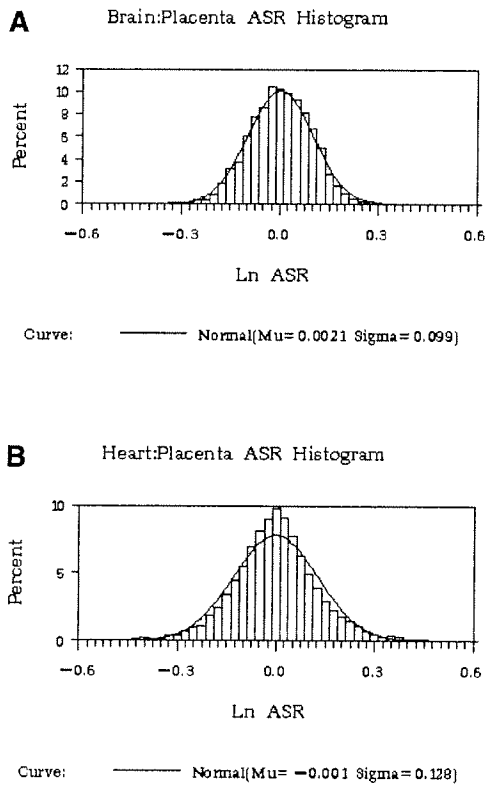

Figure 9. Histograms showing the distribution of all elements as a function of ln ASR from reciprocal labeling experiments. (**A**) Data for brain:placenta and placenta:brain hybridizations. (**B**) Data for heart:placenta and placenta:heart hybridizations.

observed for non-differentiated elements (Fig. 4B). They also had the same standard deviation. Therefore, any variation observed in DE was likely a result of real variations in experimental mRNA levels, rather than an artifact of the labeling system.

A series of independent yeast standards was also included on each microarray to assist in evaluating overall system performance. These controls demonstrated linearity in overall signal response over three orders of magnitude, a CV of 12% and a limit of detection of 2 pg mRNA at a signal-to-background ratio of 2.5 (data not shown).

CONCLUSION

In this report we have described measures important in the manufacture of cDNA microarrays and in the preparation and labeling of mRNAs for use in a two-channel hybridization system. Furthermore, the results presented in this report demonstrate in a quantitative fashion the performance of the cDNA microarray technology platform. The usefulness of any expression database is ultimately dependent on the quality of the underlying data used to construct it. We report that the cDNA microarray platform does provide the high quality data needed to establish reliable gene expression databases.

The analytical methods used to evaluate the performance of the cDNA microarray platform described in this report provide a practical framework for evaluating the performance of other technologies that purport to measure global mRNA expression. Only by disclosing the performance characteristics in a rigorous manner can researchers gauge the utility of any data produced by other platforms.

ACKNOWLEDGEMENTS

We thank the Incyte Microarray Production Facility (Fremont, CA) for manufacturing the microarrays, preparing the probes and performing the hybridizations used in this report. We also thank Drew Watson for providing resources and his encouragement to complete these experiments and Jeanne Loring for useful discussions.

REFERENCES

1. Zweiger,G. (1999) Knowledge discovery in gene-expression-microarray data: mining the information output of the genome. *Trends Biotechnol.*, **17**, 429–436.
2. Strachan,T., Abitbol,M., Davidson,D. and Beckmann,J.S. (1997) A new dimension for the human genome project: towards comprehensive expression maps. *Nat. Genet.*, **16**, 126–132.
3. Khan,J., Bittner,M.L., Chen,Y., Meltzer,P.S. and Trent,J.M. (1999) DNA microarray technology: the anticipated impact on the study of human disease. *Biochim. Biophys. Acta*, **1423**, M17–M28.
4. Marra,M., Hillier,L., Kucaba,T., Allen,M., Barstead,R., Beck,C., Blistain,A., Bonaldo,M., Bowers,Y., Bowles,L. *et al.* (1999) An encyclopedia of mouse genes. *Nat. Genet.*, **21**, 191–194.
5. Aach,J., Rindone,W. and Church,G.M. (2000) Systematic management and analysis of yeast gene expression data. *Genome Res.*, **10**, 431–445.
6. The FlyBase Consortium (1999) FlyBase, The FlyBase database of the Drosophila Genome Projects and community literature. *Nucleic Acids Res.*, **27**, 85–88.
7. Schena,M., Shalon,D., Davis,R.W. and Brown,P.O. (1995) Quantitative monitoring of gene expression patterns with a complementary DNA microarray. *Science*, **270**, 467–470.
8. Lockhart,D.J., Dong,H., Byrne,M.C., Follettie,M.T., Gallo,M.V., Chee,M.S., Mittmann,M., Wang,C., Kobayashi,M., Horton,H. and Brown,E.L. (1996) Expression monitoring by hybridization to high-density oligonucleotide arrays. *Nat. Biotechnol.*, **14**, 1675–1680.
9. Velculescu,V.E., Zhang,L, Vogelstein,B. and Kinzler,K.W. (1995) Serial analysis of gene expression. *Science*, **270**, 484–487.
10. Adams,M.D., Kelley,J.M., Gocayne,J.D., Dubnick,M., Polymeropoulos,M.H., Xiao,H., Merril,C.R., Wu,A., Olde,B., Moreno,R.F. *et al.* (1991) Complementary DNA sequencing: expressed sequence tags and human genome project. *Science*, **252**, 1651–1656.
11. Brenner,S., Johnson,M., Bridgham,J., Golda,G., Lloyd,D.H., Johnson,D., Luo,S., McCurdy,S., Foy,M., Ewan,M. *et al.* (2000) Gene expression analysis by massively parallel signature sequencing (MPSS) on microbead arrays. *Nat. Biotechnol.*, **18**, 630–634.
12. Sutcliffe,J.G., Foye,P.E., Erlander,M.G., Hilbush,B.S., Bodzin,L.J., Durham,J.T. and Hasel,K.W. (2000) TOGA: an automated parsing technology for analyzing expression of nearly all genes. *Proc. Natl Acad. Sci. USA*, **97**, 1976–1981.
13. Bartosiewicz,M., Trounstine,M., Barker,D., Johnston,R. and Buckpitt,A. (2000) Development of a toxicological gene array and quantitative assessment of this technology. *Arch. Biochem. Biophys.*, **376**, 66–73.
14. Evertsz,E., Starink,P., Gupta,R. and Watson,D. (2000) Technology and applications of gene expression microarrays. In Schena,M. (ed.), *Microarray Biochip Technology*. Eaton Publishing, Natick, MA, pp. 149–166.
15. Winzeler,E.A., Schena,M. and Davis,R.W. (1999) Fluorescence-based expression monitoring using microarrays. *Methods Enzymol.*, **306**, 3–18.
16. Hahn,G.J. and Meeker,W.Q. (1991) *Statistical Intervals: A Guide for Practioners*. John Wiley & Sons, New York.
17. Littell,R.C., Milliken,G.A., Stroup,W.W. and Wolfinger,R.D. (1996) *SAS System for Mixed Models*. SAS Institute, Cary, NC.

27 August 1999

Science

Vol. 285 No. 5432
Pages 1317–1448 $8

AMERICAN ASSOCIATION FOR THE ADVANCEMENT OF SCIENCE

VOLUME 285 27 AUGUST 1999 NUMBER 5432

Science

www.sciencemag.org

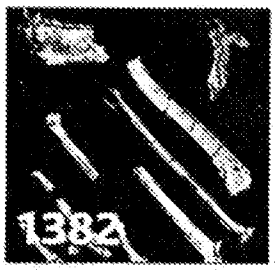

COVER Forelimb bones (longest, ~19 cm) and jaw (~8 cm) of a new partial hominoid skeleton from an ~15-million-year-old site at Kipsaramon, Kenya, superimposed on a digital elevation model of western Kenya and eastern Uganda. The skeleton represents a new genus, *Equatorius*, and will help clarify the origins of the group that includes humans and the living great apes. [Photos: Steven C. Ward]

1338
Bees do it best

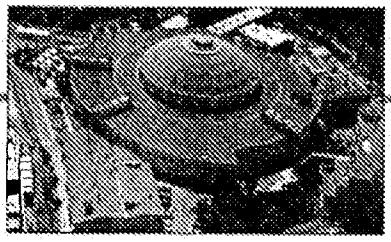

1342
A magnet for biologists

AMERICAN ASSOCIATION FOR THE ADVANCEMENT OF SCIENCE

SCIENCE (ISSN 0036-8075) is published weekly on Friday, except the last week in December, by the American Association for the Advancement of Science, 1200 New York Avenue, NW, Washington, DC 20005. Periodicals Mail postage (publication No. 484460) paid at Washington, DC, and additional mailing offices. Domestic individual membership and subscription (51 issues): $110 ($62 allocated to subscription). Domestic institutional subscription (51 issues): $325; Foreign postage extra: Mexico, Caribbean (surface mail) $55; other countries (air assist delivery) $90. First class, airmail, student, and emeritus rates on request. Canadian rates with GST available upon request, GST #1254 88122. Publications Mail Agreement Number 1069624. Printed in the U.S.A.

reached. This approach was used to estimate relative maximum leaf size during the period of study (Fig. 3).

29. The threshold for thermal damage of nonsucculent leaves (45° to 52°C) is a highly conserved characteristic across a wide range of extant taxa [W. Larcher, in *Ecophysiology of Photosynthesis*, E. D. Schultze and M. M. Caldwell, Eds. (Springer-Verlag, Berlin, 1994), pp. 261–277; Y. Gauslaa, *Holarct. Ecol.* **7**, 1 (1984)], implying little evolutionary change through time.
30. T. A. Mansfield, A. M. Hetherington, C. J. Atkinson, *Annu. Rev. Plant Physiol. Plant Mol. Biol.* **41**, 55 (1990).
31. A review of fossil Ginkgoalean leaves revealed that species with the most dissected leaves, characterized by multidichotomies 0.5 to 2 mm wide, are restricted to Late Triassic to early Middle Jurassic facies [T. Kimura, G. Naito, T. Ohana, *Bull. Natl. Sci. Mus. Tokyo* **9**, 91 (1983)].
32. The cause of T-J floral turnover has traditionally been attributed to a sedimentary hiatus (*3*). However, this hypothesis is unsupported by sedimentological evidence [G. Dam and F. Surlyk, *Geology* **20**, 749 (1992); *Spec. Publ. Int. Assoc. Sedimentol.* **18**, 4189 (1993)], which identifies no major facies changes or unconformities between the T-J strata in Greenland. Furthermore, the absence of the upper Rhaetian *Ricciisporites-Polypodisporites* acme zone [W. M. L. Schuurman, *Rev. Palaeobot. Palynol.* **23**, 159 (1977)] in Greenland (*10*) and Sweden (*11*), which has also been tentatively interpreted as evidence of a hiatus at both localities, is questionable, as acme zones are generally considered of only local use, owing to the effects of ecological, environmental, and postdepositional processes on relative pollen abundances.
33. The value of $\delta^{13}C$ is

$$\delta^{13}C = \{[(^{13}C_{unk}/^{12}C_{unk})/(^{13}C_{std}/^{12}C_{std})] - 1\} \times 1000$$

where unk the ratio of unknown to sample and std is the ratio of the pee dee belemnite standard.
34. F. M. Grandstein *et al.*, *J. Geophys. Res.* **99**, 24051 (1994).
35. We thank E. M. Friis (Swedish Museum of Natural History) and S. Funder (Danish Geological Museum) for loans and provision of fossil leaves; P. E. Olsen, F. Surlyk, W. G. Chaloner, D. J. Read, R. A. Spicer, C. K. Kelly, and P. Wignall for comments on earlier versions; and the Isotope Laboratory at Royal Holloway College, University of London, for making measurements of $\delta^{13}C$. We gratefully acknowledge funding from the Natural Environment Research Council, UK (GR9/02930), and through Royal Society Research Fellow and Equipment grants to D.J.B.

21 April 1999; accepted 26 July 1999

Gene Expression Profile of Aging and Its Retardation by Caloric Restriction

Cheol-Koo Lee,[1,3] Roger G. Klopp,[2] Richard Weindruch,[4]* Tomas A. Prolla[3]*

The gene expression profile of the aging process was analyzed in skeletal muscle of mice. Use of high-density oligonucleotide arrays representing 6347 genes revealed that aging resulted in a differential gene expression pattern indicative of a marked stress response and lower expression of metabolic and biosynthetic genes. Most alterations were either completely or partially prevented by caloric restriction, the only intervention known to retard aging in mammals. Transcriptional patterns of calorie-restricted animals suggest that caloric restriction retards the aging process by causing a metabolic shift toward increased protein turnover and decreased macromolecular damage.

Most multicellular organisms exhibit a progressive and irreversible physiological decline that characterizes senescence, the molecular basis of which remains unknown. Postulated mechanisms include cumulative damage to DNA leading to genomic instability, epigenetic alterations that lead to altered gene expression patterns, telomere shortening in replicative cells, oxidative damage to critical macromolecules by reactive oxygen species (ROS), and nonenzymatic glycation of long-lived proteins (*1*, *2*).

Genetic manipulation of the aging process in multicellular organisms has been achieved in *Drosophila* through the overexpression of catalase and Cu/Zn superoxide dismutase (*3*), in the nematode *Caenorhabditis elegans* through alterations in the insulin receptor signaling pathway (*4*), and through the selection of stress-resistant mutants in either organism (*5*). In mammals, mutations in the Werner Syndrome locus (WRN) accelerate the onset of a subset of aging-related pathology in humans (*6*), but the only intervention that appears to slow the intrinsic rate of aging is caloric restriction (CR) (*7*). Most studies have involved laboratory rodents which, when subjected to a long-term, 25 to 50% reduction in calorie intake without essential nutrient deficiency, display delayed onset of age-associated pathological and physiological changes and extension of maximum lifespan. Postulated mechanisms of action include increased DNA repair capacity, altered gene expression, depressed metabolic rate, and reduced oxidative stress (*7*).

To examine the molecular events associated with aging in mammals, we used oligonucleotide-based arrays to define the transcriptional response to the aging process in mouse gastrocnemius muscle. Our choice of tissue was guided by the fact that skeletal muscle is primarily composed of long-lived, high oxygen-consuming postmitotic cells, a feature shared with other critical aging targets such as heart and brain. Loss of muscle mass (sarcopenia) and associated motor dysfunction is a leading cause of frailty and disability in the elderly (*8*). At the histological level, aging of gastrocnemius muscle in mice is characterized by muscle cell atrophy, variations in size of muscle fibers, presence of lipofuscin deposits, collagen deposition, and mitochondrial abnormalities (*9*).

A comparison of gastrocnemius muscle from 5-month (adult) and 30-month (old) mice (*10–12*) revealed that aging is associated with alterations in mRNA levels, which may reflect changes in gene expression, mRNA stability, or both. Of the 6347 genes surveyed in the oligonucleotide microarray, only 58 (0.9%) displayed a greater than twofold increase in expression levels as a function of age, whereas 55 (0.9%) displayed a greater than twofold decrease in expression. These findings are in agreement with a differential display analysis of gene expression in tissues of aging mice (*13*). Thus, the aging process is unlikely to be due to large, widespread alterations in gene expression.

Functional classes were assigned to genes displaying the largest alterations in expression (Table 1). Of the 58 genes that increased in expression with age, 16% were mediators of stress responses, including the heat shock factors Hsp71 and Hsp27, protease Do, and the DNA damage–inducible gene GADD45 (*14*). The largest differential expression between adult and aged animals (a 3.8-fold induction) was observed for the gene encoding the mitochondrial sarcomeric creatine kinase, a critical target for ROS-induced inactivation (*15*).

A consequence of skeletal muscle aging is loss of motor neurons followed by reinnervation of muscle fibers by the remaining intact neuronal units (*16*). Genes involved in neuronal growth accounted for 9% of genes highly induced in 30-month-old animals, including neurotrophin-3 (*17*), a growth factor induced during reinnervation, and synaptic vesicle protein–2, implicated in neurite extension (*18*). PEA3, a transcriptional factor induced in the response to

[1]Environmental Toxicology Center, [2]Institute on Aging, [3]Departments of Genetics and Medical Genetics, University of Wisconsin, Madison, WI 53706, USA. [4]Department of Medicine and Wisconsin Regional Primate Research Center, University of Wisconsin, Madison, WI and Veterans Administration Hospital, Geriatric Research, Education and Clinical Center, Madison, WI 53705, USA.

*To whom correspondence should be addressed at Department of Medicine, VA Hospital (GRECC 4D), 2500 Overlook Terrace, Madison, WI 53705, USA. E-mail: rhweindr@facstaff.wisc.edu (R.W.); Departments of Genetics and Medical Genetics, 445 Henry Mall, University of Wisconsin, Madison, WI 53706, USA. E-mail: taprolla@facstaff.wisc.edu (T.A.P.)

muscle injury and previously shown to be highly expressed in muscle from old rats (*19*), was also induced in aged muscle. We also observed parallels between our results and data from fibroblasts undergoing in vitro replicative senescence. For example, HIC-5, a transcriptional factor induced by oxidative damage, and insulin-like growth factor binding protein, both associated with in vitro senescence (*20*), are induced in aged skeletal muscle.

Fifty-five (0.9%) genes displayed a greater than twofold age-related decrease in expression. Genes involved in energy metabolism accounted for 13% of these alterations (Table 1). These include alterations in genes associated with mitochondrial function and turnover, such as the adenosine 5′-triphosphate (ATP) synthase A chain and nicotinamide adenine dinucleotide phosphate (NADP) transhydrogenase genes (both involved in mitochondrial bioenergetics), the LON protease implicated in mitochondrial biogenesis, and the ERV1 gene involved in mitochondrial DNA (mtDNA) maintenance (*21*). Additionally, a decrease in metabolic activity is suggested through a decline in the expression of genes involved in glycolysis, glycogen metabolism, and the glycerophosphate shunt (Table 1).

Aging was also characterized by large reductions (twofold or more) in the expression of biosynthetic enzymes such as squalene synthase (fatty acid and cholesterol synthesis), stearoyl–coenzyme A (CoA) desaturase (polyunsaturated fatty acid synthesis), and EF-1-gamma (protein synthesis). This suppression was accompanied by a concerted decrease in the expression of genes involved in protein turnover, such as the 20*S* proteasome subunit, the 26*S* proteasome component TBP1, ubiquitin-thiolesterase, and the Unp ubiquitin-specific protease, all of which are involved in the ubiquitin-proteasome pathway of protein turnover (*22*). The directions of changes in other functional categories, such as signal transduction, and transcriptional and growth factors, did not present a consistent age-related trend.

In order to study the effects of CR on the gene expression profile of aging, we reduced caloric intake of C57BL/6 mice to 76% of that fed to control animals in early adulthood (2 months of age), and this dietary regimen was maintained until animals were killed at 30 months. A comparison of 30-month-old control and CR mice revealed that aging-related changes in gene expression profiles were remarkably attenuated by CR. Of the largest age-associated alterations (twofold or higher), 29% were completely prevented by CR and 34% were partially suppressed (Table 1). Of the four major gene classes that displayed consistent age-associated alterations, 84% were either completely or partially suppressed by CR. Thus, at the molecular level,

Table 1 (left). Aging-related changes in gene expression in gastrocnemius muscle. The extent to which caloric restriction prevented age-associated alterations in gene expression is denoted as either C (complete, >90%), N (none), or partial (20 to 90%, percentage effect indicated). The fold increase shown represents the average of all nine possible pairwise comparisons among individual mice determined by means of a specific algorithm (*12*). GenBank accession numbers are listed under ORF. A more comprehensive list that includes genes that did not fit into the six classes can be found at www1.genetics.wisc.edu/profla/Profla_Tables.html. **Table 2 (right).** Caloric restriction–induced alterations in gene expression. The data represent a comparison between 30-month-old CR-fed and control-fed mice. The gene expression alterations listed in this Table are diet related and do not include those representing prevention of age-associated changes (see Table 1). Additional CR-induced changes are posted at the aforementioned Web site.

ORF	Δ Age (fold)	Gene	Function	CR Prevention
W08057	↑ 3.5	Heat Shock 27 kDa Protein	Chaperone	C
M17790	↑ 3.5	Serum Amyloid A Isoform 4	Unknown	N
AA114576	↑ 3.4	Heat Shock 71 kDa Protein	Chaperone	C
L28177	↑ 2.6	GADD45	DNA damage response	77%
M74570	↑ 2.4	Aldehyde Dehydrogenase II	Aldehyde detoxification	29%
AA059662	↑ 2.2	Protease Do Precursor	Protease	C
L22482	↑ 2.2	HIC-5	Senescence and differentiation	C
X99963	↑ 2.2	rhoB	Unknown	87%
X65627	↑ 2.1	TNZ2	RNA metabolism	64%
X57277	↑ 1.8	Rac1	JNK activator	C
AA071777	↑ 3.8	Synaptic Vesicle Protein 2	Neurite extension	51%
X53257	↑ 2.5	Neurotrophin-3	Reinnervation of muscle	50%
X78197	↑ 2.2	AP-2 Beta	Neurogenesis	N
X89749	↑ 2.1	mTGIF	Differentiation	C
AA014024	↑ 2.1	Dynactin	Transport	55%
X63190	↑ 2.1	PEA3	Response to muscle injury	C
AA106112	↑ 3.8	Mitochondrial Sarcomeric Creatine Kinase	ATP generation	C
AA061886	↑ 2.0	Dihydropyridine-sensitive L-type Calcium Channel	Calcium channel	67%
AA061310	↓ 4.1	Mitochondrial LON Protease	Mitochondrial biogenesis	C
W55037	↓ 2.9	Alpha Enolase	Glycolysis	68%
V00719	↓ 2.6	Alpha-Amylase-1	Carbohydrate metabolism	N
M81475	↓ 2.5	Phosphoprotein Phosphatase	Glycogen metabolism	C
AA034842	↓ 2.1	ERV1	mtDNA maintenance	46%
AA106406	↓ 2.0	ATP Synthase A Chain	ATP synthesis	N
AA041826	↓ 2.0	IPP-2	Glycogen metabolism	C
L27842	↓ 2.0	PMP35	Peroxisome assembly	60%
Z49204	↓ 2.0	NADP Transhydrogenase	Glycerophosphate shunt	N
AA071776	↓ 1.9	Glucose-6-Phosphate Isomerase	Glycolysis	C
M13366	↓ 1.9	Glycerophosphate Dehydrogenase	Glycerophosphate shunt	C
AA107752	↓ 2.9	EF-1-Gamma	Protein synthesis	63%
U22031	↓ 2.6	20S Proteasome Subunit	Protein turnover	44%
AA061604	↓ 2.2	Ubiquitin Thiolesterase	Protein turnover	C
AA145829	↓ 2.1	26S Proteasome Component TBP1	Protein turnover	C
L00681	↓ 2.1	Unp Ubiquitin Specific Protease	Protein turnover	N
U35741	↓ 2.0	Rhodanese	Mitochondrial protein folding	C
D83585	↓ 1.7	Proteasome Z Subunit	Protein turnover	C
D76440	↓ 2.9	Necdin	Neuronal growth suppressor	47%
X75014	↓ 2.7	Phox2 Homeodomain Protein	Trophic factor	65%
M32240	↓ 2.1	GAS3	Myelin protein	55%
M16465	↓ 3.4	Calpactin I Light Chain	Calcium effector	C
L34611	↓ 2.3	PTHR	Calcium homeostasis	N
AA103356	↓ 2.2	Calmodulin	Calcium effector	N
D29016	↓ 6.4	Squalene Synthase	Cholesterol/fatty acid synthesis	52%
M21285	↓ 2.1	Stearoyl-CoA Desaturase	PUFA synthesis	C
U73744	↓ 2.1	HSP70	Chaperone	N

Energy Metabolism · Protein Metabolism · Biosynthesis · Neuronal Factors · Stress Response · Calcium Metabolism

ORF	Δ CR (fold)	Gene	Function
U05809	↑ 4.5	Transketolase	Pentose phosphate pathway
W53351	↑ 4.1	Fructose-bisphosphate Aldolase	Glycolysis/Gluconeogenesis
AA071776	↑ 3.5	Glucose-6-Phosphate Isomerase	Glycolysis/Gluconeogenesis
U34295	↑ 2.3	Glucose Dependent Insulinotropic Polypeptide	Insulin sensitizer
U01841	↑ 2.3	Peroxisome Proliferator Receptor Gamma	Insulin sensitizer
L28116	↑ 2.0	PPAR Delta	Peroxisome induction
D42083	↑ 1.9	Fructose 1,6-bisphosphatase	Gluconeogenesis
AA041826	↑ 1.9	Protein Phosphatase Inhibitor 2 (IPP-2)	Inhibition of glycogen synthesis
U37091	↑ 1.8	Carbonic Anhydrase IV	CO_2 disposal
M13366	↑ 1.8	Glycerophosphate Dehydrogenase	Electron transport to mitochondria
AA119868	↑ 1.7	Pyruvate Kinase	Glycolysis
AA145829	↑ 2.3	26S Protease Subunit TBP-1	Protein turnover
AA107752	↑ 2.2	Elongation Factor 1-gamma	Protein synthesis
W53731	↑ 2.1	Signal Recognition Receptor Alpha Subunit	Protein synthesis
U60328	↑ 2.1	Proteasome Activator PA28 Alpha Subunit	Protein turnover
X59990	↑ 2.0	mCyP-S1 (Cyclophilin)	Protein folding
W08293	↑ 1.9	Translocon-Associated Protein Delta	Protein translocation
W57495	↑ 1.8	60S Ribosomal Protein L23	Protein synthesis
X13135	↑ 4.7	Fatty Acid Synthase	Fatty acid synthesis
X16314	↑ 2.5	Glutamine Synthetase	Glutamine synthesis
AA137659	↑ 2.4	Cytochrome P450-IIC12	Steroid biosynthesis
L32973	↑ 2.0	Thymidylate Kinase	dTTP synthesis
X56548	↑ 2.0	Purine Nucleoside Phosphorylase	Purine turnover
AA022083	↑ 2.0	Huntingtin	Unknown
D76440	↑ 1.9	Necdin	Growth suppressor
AA062328	↓ 3.4	DnaJ Homolog 2	Chaperone
X63023	↓ 1.9	Cytochrome P-450-IIIA	Detoxification
U03283	↓ 1.8	Cyp1b1 Cytochrome P450	Detoxification
U14390	↓ 1.8	Aldehyde Dehydrogenase-3	Detoxification
X76850	↓ 1.8	MAPKAP2	Unknown
D26123	↓ 1.7	Carbonyl Reductase	Detoxification
L4406	↓ 1.7	Hsp105-beta	Chaperone
U40930	↓ 1.5	Oxidative Stress-Induced Protein	Unknown
U66887	↓ 1.8	RAD50	Double strand break repair
AA059718	↓ 1.7	DNA Polymerase Beta	Base excision repair
W42234	↓ 1.6	XPE	Nucleotide excision repair
D43694	↓ 1.8	Math-1	Differentiation
D16464	↓ 1.7	HES-1	Differentiation
W13191	↓ 1.6	Thyroid Hormone Receptor Alpha-2	Thyroid hormone receptor

Energy Metabolism · Protein Metabolism · Biosynthesis · Neuronal Factors · Stress Response · DNA Repair

CR mice appear to be biologically younger than animals receiving the control diet.

Caloric restriction induced a metabolic reprogramming characterized by a transcriptional shift toward energy metabolism, increased biosynthesis, and protein turnover (Table 2). CR resulted in the induction of 51 genes (1.8-fold or higher) as compared with age-matched animals consuming the control diet. Nineteen percent of genes in this class are related to energy metabolism. Modulation of energy metabolism was evident through the induction of glucose-6-phosphate isomerase (glycolysis), fructose 1,6-bisphosphatase (gluconeogenesis), IPP-2 (an inhibitor of glycogen synthesis), and transketolase. Fructose 1,6-bisphosphatase switches the direction of a key regulatory step in glycolysis toward a biosynthetic precursor, glucose-6-phosphate. Remarkably, this same adaptation has been observed as part of the transcriptional reprogramming of *Saccharomyces cerevisiae* accompanying the diauxic switch from anaerobic growth to aerobic respiration upon depletion of glucose (*23*). Transketolase, which controls the nonoxidative branch of the pentose phosphate pathway, provides NADPH for biosynthesis and reducing power for several antioxidant systems. CR also induced transcripts associated with fatty acid metabolism, such as fatty acid synthase and PPAR-delta, a mediator of peroxisome proliferation. Interestingly, CR may act to increase insulin sensitivity through the induction of glucose-dependent insulinotropic peptide and PPAR-gamma, a potent insulin sensitizer (*24*).

Biosynthetic ability also appears to be induced in CR mice. CR up-regulated the expression of glutamine synthase, purine nucleoside phosphorylase (purine turnover), and thymidylate kinase (dTTP synthesis). Remarkably, 16% of transcripts highly induced by CR encode proteins involved in protein synthesis and turnover, including elongation factor 1-gamma, proteasome activator PA28, translocon-associated protein delta, 60*S* ribosomal protein L23, and the 26*S* proteasome subunit TBP-1.

CR was associated with a 1.6-fold or greater reduction in expression of 57 genes. Of these, 12% were associated with stress responses or DNA repair pathways, or both (Table 2). Among the 6347 genes examined, the most substantial suppression of gene expression by CR was for a murine DnaJ homolog (3.4-fold), a pivotal and inducible heat shock factor that senses and transduces the presence of misfolded or damaged proteins in bacteria (*25*). CR also lowered the expression of cytochrome P450 isoforms IIIA and Cyp1b1 (involved in detoxification), Hsp105 (a heat shock factor), aldehyde dehydrogenase (an inducible enzyme involved in detoxification of metabolic by-products), and an oxidative stress–induced protein of unknown function. CR reduced the expression of several DNA repair genes including XPE (a factor that recognizes multiple DNA adducts), RAD50 (involved in double-strand break repair), and DNA polymerase–beta (a DNA damage–inducible polymerase). We also find molecular evidence to support a state of lower basal metabolic rate in CR mice through lowered expression of the thyroid-hormone receptor alpha gene (*26*).

The data presented here provide the first global assessment of the aging process in mammals at the molecular level and underscore the utility of large-scale, parallel gene expression analysis in the study of complex biological phenomena. We estimate that the 6347 genes analyzed in this study represent 5 to 10% of the mouse genome. Additional classes of aging-related genes in skeletal muscle may be discovered with the development of higher density mammalian DNA microarrays. The observed collection of gene expression alterations in aging skeletal muscle is complex, reflecting the presence of myocyte, neuronal, and vascular components. Although some of the age-associated alterations in gene expression could represent maturational changes, this possibility is unlikely given the fact that the 5-month-old (adult) mice used in this study were fully mature animals. Importantly, changes in mRNA levels may not always result in a parallel alteration in protein levels. However, the complete or partial prevention of most age-related alterations by CR suggests that gene expression profiles can be used to assess the biological age of mammalian tissues, providing a tool for evaluating experimental interventions.

Taken as a whole, our results provide evidence that during aging there is an induction of a stress response as a result of damaged proteins and other macromolecules. This response ensues as the systems required for the turnover of such molecules decline, perhaps as a result of an energetic deficit in the cell. In particular, the observed alterations in transcripts associated with energy metabolism and mitochondrial function may reflect either decreased mitochondrial biogenesis or turnover secondary to cumulative ROS-inflicted mitochondrial damage (*2*), lending support to the concept that mitochondrial dysfunction plays a central role in aging of postmitotic tissues. The gene expression profile also suggests that secondary responses to the aging process in skeletal muscle involve the activation of neuronal and myogenic responses to injury.

A summary of global changes induced by aging, and the contrasting effects of CR, are shown in Table 3. The transcriptional activation of stress response genes that process damaged or misfolded proteins during aging, and the prevention of this induction by CR, suggest a central role for protein modifications in aging. Indeed, aging is characterized by an exponential increase of oxidatively damaged proteins (*27*). Previous analyses of metabolic rates in CR animals have led to the suggestion that this life-extending regimen acts through a reduction in metabolic rate, resulting in a lower production of toxic by-products of metabolism (*28*). The CR-mediated reduction of mRNAs encoding inducible genes involved in metabolic detoxification, DNA repair, and the response to oxidative stress supports this view, because it implies lower substrate availability for these systems. Additionally, our analysis indicates that CR may cause a metabolic shift toward increased biosynthesis and macromolecular turnover. A hormonal trigger for this shift may be an alteration in the insulin signaling pathway through increased expression of genes that mediate insulin sensitivity, a finding that links our observations to those obtained through the genetic analysis of aging in the nematode *C. elegans* (*4*).

Table 3. Global view of transcriptional changes induced by aging and caloric restriction.

Aging	Caloric restriction
↑ **Stress response** Induction of: Heat shock response DNA damage–inducible genes Oxidative stress–inducible genes	↑ **Protein metabolism** Increased synthesis Increased turnover
↓ **Energy metabolism** Reduced glycolysis Mitochondrial dysfunction	↑ **Energy metabolism** Up-regulation of gluconeogenesis, and the pentose phosphate shunt
↑ **Neuronal injury** Reinnervation Neurite extension and sprouting	↑ **Biosynthesis** Fatty acid synthesis Nucleotide precursors
	↓ **Macromolecular damage** Suppression of: Inducible heat shock factors Inducible detoxification systems Inducible DNA repair systems

References and Notes

1. S. M. Jazwinski, *Science* **273**, 54 (1996); G. M. Martin, S. N. Austad, T. E. Johnson, *Nature Genet.* **13**, 25 (1996); F. B. Johnson, D. A. Sinclair, L. Guarente, *Cell* **96**, 291 (1996).

2. K. B. Beckman and B. N. Ames, *Physiol. Rev.* **78**, 547 (1998).
3. W. C. Orr and R. S. Sohal, *Science* **263**, 1128 (1994); T. L. Parkes *et al.*, *Nature Genet.* **19**, 171 (1998).
4. S. Ogg *et al.*, *Nature* **389**, 994 (1997); K. Lin, J. B. Dorman, A. Rodan, C. Kenyon, *Science* **278**, 1319 (1997); S. Paradis and G. Ruvkun, *Genes Dev.* **12**, 2488 (1998); H. A. Tissenbaum and G. Ruvkun, *Genetics* **148**, 703 (1998).
5. T. E. Johnson, *Science* **249**, 908 (1990); S. Murakami and T. E. Johnson, *Genetics* **143**, 1207 (1996); Y.-J. Lin, L. Seroude, S. Benzer, *Science* **282**, 943 (1998).
6. C. E. Yu *et al.*, *Science* **272**, 258 (1996); L. Ye *et al.*, *Am. J. Med. Genet.* **68**, 494 (1997).
7. R. Weindruch and R. L. Walford, *The Retardation of Aging and Disease by Dietary Restriction* (Thomas, Springfield, IL, 1988).
8. C. Dutta, E. C. Hadley, J. Lexell, *Muscle Nerve* **5**, S5 (1997).
9. R. Ludatscher, M. Silberman, D. Gershon, A. Reznick, *Exp. Gerontol.* **18**, 113 (1983).
10. Methods used to house and feed male C57BL/6 mice, a commonly used model in aging research with an average life-span of ~30 months, were recently described [T. D. Pugh, T. D. Oberley, R. Weindruch, *Cancer Res.* **59**, 642 (1999)].
11. Total RNA was extracted from frozen tissue by using TRIZOL reagent (Life Technologies). Polyadenylate [poly(A)$^+$] RNA was purified from the total RNA with oligo-dT–linked Oligotex resin (Qiagen). One microgram of poly(A)$^+$ RNA was converted into double-stranded cDNA (ds-cDNA) by using SuperScript Choice System (Life Technologies) with an oligo-dT primer containing a T7 RNA polymerase promoter (Genset). After second-strand synthesis, the reaction mixture was extracted with phenol–chloroform–isoamyl alcohol, and ds-cDNA was recovered by ethanol precipitation. In vitro transcription was performed by using a T7 Megascript Kit (Ambion) with 1.5 μl of ds-cDNA template in the presence of a mixture of unlabeled ATP, CTP, GTP, and UTP and biotin-labeled CTP and UTP [bio-11-CTP and bio-16-UTP (Enzo)]. Biotin-labeled cRNA was purified by using an RNeasy affinity column (Qiagen), and fragmented randomly to sizes ranging from 35 to 200 bases by incubating at 94°C for 35 min. The hybridization solutions contained 100 mM MES, 1 M Na$^+$, 20 mM EDTA, and 0.01% Tween 20. The final concentration of fragmented cRNA was 0.05 μg/μl in the hybridization solutions. After hybridization, the hybridization solutions were removed and the gene chips were washed and stained with streptavidin-phycoerythrin. DNA chips were read at a resolution of 6 μm with a Hewlett-Packard GeneArray Scanner.
12. Detailed protocols for data analysis of Affymetrix microarrays and extensive documentation of the sensitivity and quantitative aspects of the method have been described [D. J. Lockhart, *Nature Biotechnol.* **14**, 1675 (1996)]. Briefly, each gene is represented by the use of ~20 perfectly matched (PM) and mismatched (MM) control probes. The MM probes act as specificity controls that allow the direct subtraction of both background and cross-hybridization signals. The number of instances in which the PM hybridization signal is larger than the MM signal is computed along with the average of the logarithm of the PM:MM ratio (after background subtraction) for each probe set. These values are used to make a matrix-based decision concerning the presence or absence of an RNA molecule. Positive average signal intensities after background subtraction were observed for over 4000 genes for all samples. To determine the quantitative RNA abundance, the average of the differences representing PM minus MM for each gene-specific probe family is calculated, after discarding the maximum, the minimum, and any outliers beyond 3 SDs. Averages of pairwise comparisons were made between animals with Affymetrix software. To determine the effect of age, each 5-month-old mouse (n = 3) was compared to each 30-month-old (n = 3) mouse, generating a total of nine pairwise comparisons. To determine the effect of diet, 30-month-old CR-fed (n = 3) and 30-month-old control-fed (n = 3) animals were similarly compared. Pearson correlation coefficients were calculated between individual animals in the same age/diet groups. No correlation coefficient between two animals in the same age/diet group was less than 0.98.
13. M. H. Goyns *et al.*, *Mech. Ageing Dev.* **101**, 73 (1998).
14. J. Jackman, I. Alamo Jr., A. J. Fornace Jr., *Cancer Res.* **54**, 5656 (1994).
15. O. Stachowiak, M. Dolder, T. Wallimann, C. Richter, *J. Biol. Chem.* **273**, 16694 (1998).
16. L. Larsson, *J. Gerontol. Biol. Sci.* **50A**, 96 (1995); J. Lexell, *J. Nutr.* **127**, 1011S (1997).
17. J. C. Copray and N. Brouwer, *Neurosci. Lett.* **236**, 41 (1997).
18. G. Marazzi and K. M. Buckley, *Dev. Dyn.* **197**, 115 (1993).
19. C. A. Peterson and J. D. Houle, *J. Nutr.* **127**, 1007S (1997).
20. M. Shibanuma, J. Mashimo, T. Kurokl, K. Nose, *J. Biol. Chem.* **269**, 26767 (1994); S. Wang, E. J. Moerman, R. A. Jones, R. Thweatt, S. Goldstein, *Mech. Ageing Dev.* **92**, 121 (1996).
21. ATP synthase: W. Junge, H. Lill, S. Engelbrecht, *Trends Biochem. Sci.* **22**, 420 (1997); NADP transhydrogenase: J. B. Hoek and J. Rydstrom, *Biochem. J.* **254**, 1 (1988); LON protease: K. Luciakova, B. Sokolikova, M. Chloupkova, B. D. Nelson, *FEBS Lett.* **444**, 186 (1999); ERV1: T. Lisowsky, *Curr. Genet.* **26**, 15 (1994).
22. A. L. Schwartz and A. Ciechanover, *Annu. Rev. Med.* **50**, 57 (1999).
23. J. L. DeRisi, V. R. Iyer, P. O. Brown, *Science* **278**, 680 (1997).
24. J. R. Zierath *et al.*, *Endocrinology* **139**, 5034 (1998).
25. T. Tomoyasu, T. Ogura, T. Tatsuta, B. Bukau, *Mol. Microbiol.* **30**, 567 (1998); T. Yura, H. Nagai, H. Mori, *Annu. Rev. Microbiol.* **47**, 321 (1993).
26. L. Wikstrom *et al.*, *EMBO J.* **17**, 455 (1998).
27. E. R. Stadtman, *Science* **257**, 1220 (1992).
28. R. S. Sohal and R. Weindruch, *ibid.* **273**, 59 (1996).
29. Supported by NIH grants PO1 AG11915 (R.W.) and RO1 CA78723 (T.A.P.). T.A.P. is a recipient of the Shaw Scientist (Milwaukee Foundation) and Burroughs Wellcome Young Investigator awards.

19 May 1999; accepted 22 July 1999

Dual Function of the Selenoprotein PHGPx During Sperm Maturation

Fulvio Ursini,[1] Sabina Heim,[2] Michael Kiess,[2] Matilde Maiorino,[1] Antonella Roveri,[1] Josef Wissing,[2] Leopold Flohé[3]*

The selenoprotein phospholipid hydroperoxide glutathione peroxidase (PHGPx) changes its physical characteristics and biological functions during sperm maturation. PHGPx exists as a soluble peroxidase in spermatids but persists in mature spermatozoa as an enzymatically inactive, oxidatively cross-linked, insoluble protein. In the midpiece of mature spermatozoa, PHGPx protein represents at least 50 percent of the capsule material that embeds the helix of mitochondria. The role of PHGPx as a structural protein may explain the mechanical instability of the mitochondrial midpiece that is observed in selenium deficiency.

Selenium is essential for male fertility in rodents and has also been implicated in the fertilization capacity of spermatozoa of livestock and humans (*1*). Selenium deficiency is associated with impaired sperm motility, structural alterations of the midpiece, and loss of flagellum (*1*). However, three decades after the discovery of selenium as an integral constituent of redox enzymes (*2*), the molecular basis of the relationship of the essential trace element and male fertility remains obscure. The selenoprotein PHGPx (Enzyme Commission number 1.11.1.12) is abundantly expressed in spermatids and displays high activity in postpubertal testis (*3*). In mature spermatozoa, however, selenium is largely restricted to the mitochondrial capsule, a keratin-like matrix that embeds the helix of mitochondria in the sperm midpiece (*4*). A "sperm mitochondria–associated cysteine-rich protein (SMCP)" (*5*) had been considered to be the selenoprotein accounting for the selenium content of the mitochondrial capsule (*4*–*6*). The rat SMCP gene, however, does not contain an in-frame TGA codon (*7*) that would enable a selenocysteine incorporation (*8*). In mice, the three in-frame TGA codons of the SMCP gene are upstream of the translation start (*5*). SMCP can therefore no longer be considered as a selenoprotein. Instead, the "mitochondrial capsule selenoprotein (MCS)," as SMCP was originally referred to (*4*–*7*), is here identified as PHGPx.

Routine preparations of rat sperm mitochondrial capsules (*9*) yielded a fraction that was insoluble in 1% SDS containing 0.2 mM dithiothreitol (DTT) and displayed a vesicular appearance in electron microscopy (Fig. 1A). The vesicles readily disintegrated upon exposure to 0.1 M mercaptoethanol (Fig. 1B) and became fully soluble in 6 M guanidine-HCl. When the solubilized capsule material was subjected to polyacrylamide gel electrophoresis (PAGE), four bands in the 20-kD

[1]Dipartmento di Chimica Biologica, Università di Padova, Viale G. Colombo 3, I-35121 Padova, Italy. [2]National Research Centre for Biotechnology (GBF), Mascheroder Weg 1, D-38124 Braunschweig, Germany. [3]Department of Biochemistry, Technical University of Braunschweig, Mascheroder Weg 1, D-38124 Braunschweig, Germany.

*To whom correspondence should be addressed. E-mail: lfl@gbf.de

Molecular Cancer

BioMed Central

Research

Open Access

Gene expression profiling by DNA microarray analysis in mouse embryonic fibroblasts transformed by ras^{V12} mutated protein and the E1A oncogene

Sophie Vasseur[1], Cédric Malicet[1], Ezequiel L Calvo[2], Claude Labrie[2], Patrice Berthezene[1], Jean Charles Dagorn[1] and Juan Lucio Iovanna*[1]

Address: [1]Centre de Recherche INSERM EMI 0116, 163 Avenue de Luminy, BP172, 13009 Marseille, France and [2]Molecular Endocrinology and Oncology Research Center, Laval University Medical Center 2705 Laurier Boulevard, Quebec, G1V 4G2, Canada

Email: Sophie Vasseur - vasseur@marseille.inserm.fr; Cédric Malicet - malicet@marseille.inserm.fr; Ezequiel L Calvo - ecalvo@crchul.ulaval.ca; Claude Labrie - claude.labrie@crchul.ulaval.ca; Patrice Berthezene - berthezene@marseille.inserm.fr; Jean Charles Dagorn - dagorn@marseille.inserm.fr; Juan Lucio Iovanna* - iovanna@marseille.inserm.fr

* Corresponding author

Published: 19 March 2003

Molecular Cancer 2003, **2**:19

Received: 24 January 2003
Accepted: 19 March 2003

This article is available from: http://www.molecular-cancer.com/content/2/1/19

Abstract

Background: Ras is an area of intensive biochemical and genetic studies and characterizing downstream components that relay ras-induced signals is clearly important. We used a systematic approach, based on DNA microarray technology to establish a first catalog of genes whose expression is altered by ras and, as such, potentially involved in the regulation of cell growth and transformation.

Results: We used DNA microarrays to analyze gene expression profiles of ras^{V12}/E1A-transformed mouse embryonic fibroblasts. Among the ~12,000 genes and ESTs analyzed, 815 showed altered expression in ras^{V12}/E1A-transformed fibroblasts, compared to control fibroblasts, of which 203 corresponded to ESTs. Among known genes, 202 were up-regulated and 410 were down-regulated. About one half of genes encoding transcription factors, signaling proteins, membrane proteins, channels or apoptosis-related proteins was up-regulated whereas the other half was down-regulated. Interestingly, most of the genes encoding structural proteins, secretory proteins, receptors, extracellular matrix components, and cytosolic proteins were down-regulated whereas genes encoding DNA-associated proteins (involved in DNA replication and reparation) and cell growth-related proteins were up-regulated. These data may explain, at least in part, the behavior of transformed cells in that down-regulation of structural proteins, extracellular matrix components, secretory proteins and receptors is consistent with reversion of the phenotype of transformed cells towards a less differentiated phenotype, and up-regulation of cell growth-related proteins and DNA-associated proteins is consistent with their accelerated growth. Yet, we also found very unexpected results. For example, proteases and inhibitors of proteases as well as all 8 angiogenic factors present on the array were down-regulated in transformed fibroblasts although they are generally up-regulated in cancers. This observation suggests that, in human cancers, proteases, protease inhibitors and angiogenic factors could be regulated through a mechanism disconnected from ras activation.

Conclusions: This study established a first catalog of genes whose expression is altered upon fibroblast transformation by ras^{V12}/E1A. This catalog is representative of the genome but not exhaustive, because only one third of expressed genes was examined. In addition, contribution to ras signaling of post-transcriptional and post-translational modifications was not addressed. Yet, the information gathered should be quite useful to future investigations on the molecular mechanisms of oncogenic transformation.

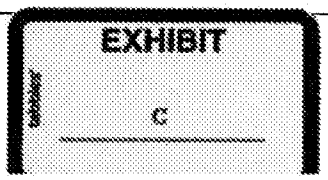

Background

Cancer is a disease caused by multiple genetic alterations that lead to uncontrolled cell proliferation. This process often involves activation of cellular proto-oncogenes and inactivation of tumour-suppressor genes. One of the earliest and most potent oncogenes identified in human cancer is the mutant *ras* [1,2]. *Ras* family of proto-oncogenes encodes small GTP-binding proteins that transduce mitogenic signals from tyrosine-kinase receptors [reviewed in [3]]. *In vitro*, oncogenic *ras* efficiently transforms most immortalized rodent cell lines but fails to transform mouse primary cells [4]. However, *ras* can transform primary mouse cells by cooperating with other oncogenic alterations such as overexpression of c-Myc, dominant negative p53, D-type cyclins, Cdc25A and Cdc25B, or loss of *p53*, *p16* or *IRF-1* [5–7]. Several viral onco-proteins can also cooperate with *ras*, for example SV40 T-antigen, adenovirus E1A, human papillomavirus E7 and HTLV-1 Tax [reviewed in [6,7]]. When expressed alone in primary cells, most of these alterations facilitate their immortalization [7]. Oncogenic transformation of primary cells by co-expression of *ras* and immortalizing mutations constitutes a model of multistep tumorigenesis that has been reproduced in animal systems [reviewed in [8,9]].

Ras has been an area of intensive biochemical and genetic studies [10]. These studies helped to characterize downstream signaling events and components that relay *ras*-induced mitogenic signals to the ultimate transcription factors which regulate expression of genes involved in cell growth and transformation. Downstream signaling elicited by the oncogenic form of Ras protein impairs regulation of gene expression with eventual disruption of normal cellular functions. Downstream transcription factors were found essential for *ras*-mediated cell transformation [11–13]. However, compared with our knowledge on *ras* signaling events, little is known on target genes involved in the phenotypic changes resulting from *ras* activation, such as cell transformation. Thus, identification of genes whose expression is altered during *ras*-mediated cell transformation would provide important information on the underlying molecular mechanism. In the present work, we used DNA microarray technology to analyze gene expression profiles of ras^{V12}/E1A-transformed primary mouse embryonic fibroblasts (MEFs), in order to identify genes whose expression is transformation-dependent.

Results

Analysis of gene expression changes after ras^{V12}/E1A-transformation

We used microarray analysis to compare expression profiles of ~12,000 genes in normal vs. ras^{V12}/E1A-transformed fibroblasts. Figure 1 shows the phenotypic changes of the ras^{V12}/E1A-transformed MEFs. With Affymetrix microarray technology, differential expression values greater than 1.7 are likely to be significant, based on internal quality control data. We present data which use a more stringent ratio, restricting our analysis to genes that are overexpressed or under-expressed at least 2.0 fold in ras^{V12}/E1A-transformed fibroblasts relative to the empty retrovirus-transduced MEFs. We summarize the highlights below and present the full profile in Figure 2.

Among the ~12,000 genes and ESTs analyzed, expression of 815 showed to be altered by at least 2.0 fold in the ras^{V12}/E1A-transformed fibroblasts, of which 203 corresponded to ESTs. Among known genes, 202 were up-regulated (Table 1)(see Additional file 1) whereas 410 were down-regulated (Table 2)(see Additional file 2) by ras^{V12}/E1A-transformation. It is interesting to note that about one half of genes encoding transcription factors, signaling proteins, membrane proteins, channels, or apoptosis-related proteins was up-regulated whereas the other half was down-regulated (Figure 2). However, after ras^{V12}/E1A-transformation most of genes encoding structural proteins, secretory proteins, receptors, proteases, protease inhibitors, extracellular matrix components, proteins involved in angiogenesis and cytosolic proteins, were down-regulated whereas genes encoding DNA-associated proteins (involved in DNA replication and reparation) and cell growth-related proteins were up-regulated (Figure 2). These data may explain, at least in part, the behavior of transformed cells. For example, down-regulation of structural proteins, extracellular matrix components, secretory proteins and receptors is consistent with reversion of the phenotype of transformed cells towards a less differentiated phenotype and up-regulation of cell growth-related proteins and DNA-associated proteins is consistent with their accelerated growth.

Transcription factors

57 genes encoding transcription factors were up-regulated and 45 down-regulated by ras^{V12}/E1A-transformation. The most strongly activated genes corresponded to the homeobox protein SPX1 (39 fold), myb proto-oncogene (25 fold) and the paired-like homeodomain transcription factor (19 fold), whereas the most repressed were the osteoblast specific factor 2 (123 fold), the p8 protein (51 fold), the H19 mRNA (21 fold) and the early B-cell factor (20 fold).

Structural proteins

Expressions of 10 genes encoding structural proteins were up-regulated in MEFs-transformed cells, 44 being down-regulated. The most important up-regulation was observed for cytokeratin (26 fold) and desmoplakin I (17 fold), the strongest down-regulations for smooth muscle calponin (115 fold), transgelin (49 fold), debrin (41

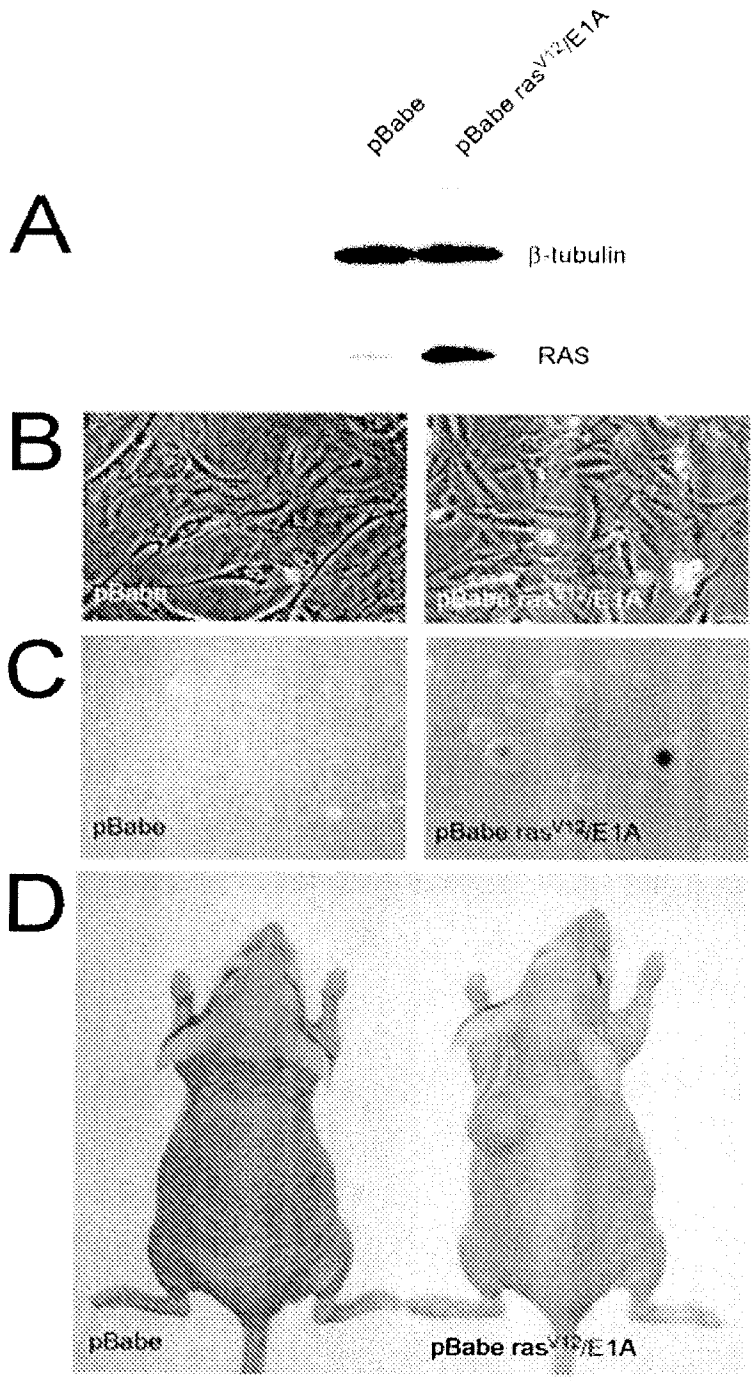

Figure 1

A. Expression of RAS was verified by immunoblot analysis in MEFs transduced with pBabe (control) or pBabe-ras^{V12}/E1A (transformed) retroviruses. B. Morphological aspect of the pBabe and pBabe-ras^{V12}/E1A transduced mouse embryonic fibroblats. C. Anchorage-independent growth of the ras^{V12}/E1A transformed MEF. Fifty thousand cells were plated on 0.6% agar in DMEM-10% FCS and overlaid on 0.6% agar in the same medium. Photomicrographs were taken 10 days after plating. D. ras^{V12}/E1A transformed MEF induce tumor formation. One million of pBabe and pBabe-ras^{V12}/E1A transduced mouse embryonic fibroblast were injected in 200 μl PBS as xenografts in nude mice. Representative mice at day 18.

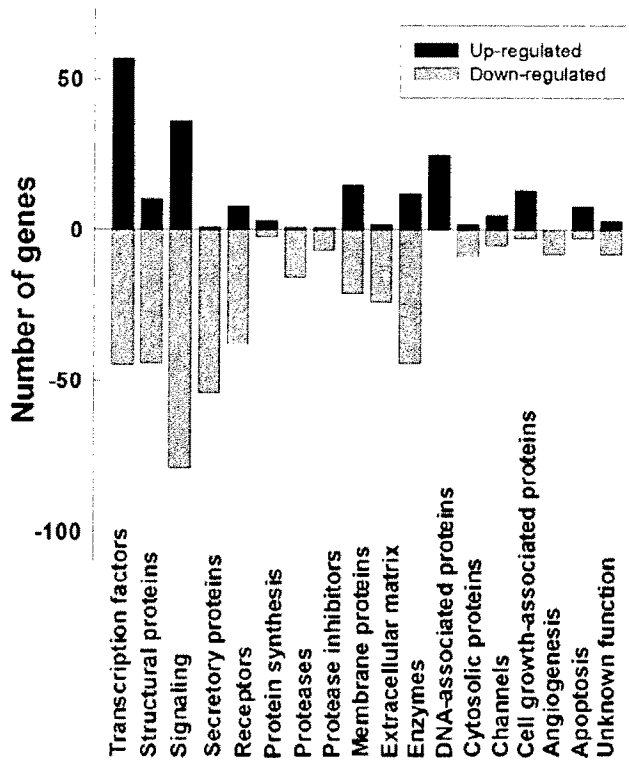

Figure 2
Gene expression changes after ras^{V12}/E1A-transformation. Number of genes up-regulated or down-regulated were grouped by function (Transcription factors, structural proteins, signaling, secretory proteins, receptors, protein synthesis, proteases, protease inhibitors, membrane proteins, extracellular matrix, enzymes, DNA-associated proteins, cytosolic proteins, channels, cell growth-associated proteins, angiogenesis, apoptosis and unknown function). Bars represent the number of genes in each group.

fold), p50b (35 fold) and vascular smooth muscle alpha-actin (34 fold).

Signaling factors
36 genes encoding proteins involved in numerous signaling pathways were up-regulated and 79 down-regulated in ras^{V12}/E1A-transformed MEFs. The EGP314 precursor (also known as the calcium signal transducer 1) was found 25 fold up-regulated, whereas the cysteine rich intestinal protein (41 fold) and ASM-like phosphodiesterase 3a (31 fold) were the most strongly down-regulated genes.

Secretory proteins
Only one gene, encoding the transforming growth factor alpha, was detected as up-regulated (3 fold) in transformed cells. By contrast, expressions of 54 secretory proteins were repressed after ras^{V12}/E1A-transformation. The most affected genes were those encoding cholecystokinin (112 fold), serum amyloid A3 (85 fold), PRDC (58 fold), insulin-like growth factor binding protein 5 (41 fold), gremlin (36 fold), follistatin (33 fold), the small inducible cytokine subfamily B (27 fold), cytokine SDF-1-beta (23 fold) and the small inducible cytokine A7 (22 fold).

Receptors
8 receptors were up-regulated and 38 down-regulated in transformed fibroblasts. Overexpression was observed for acetylcholine receptor beta (8 fold), tyrosine kinase receptor (3 fold), growth hormone releasing hormone receptor (3 fold), semaphorin M-sema G (3 fold) and amphiregulin (2 fold). Strongest down-regulations were found for integrin alpha 5 (43 fold), transient receptor protein 2 (19 fold), retinoic acid receptor alpha (14 fold), retinoic orphan receptor 1 (11 fold) and platelet derived growth factor receptor (12 fold).

Protein synthesis
3 genes involved in protein synthesis (BRIX, nucleolin, ribosomal protein L44 and SIK similar protein) were overexpressed and 2 (ribosomal protein S4X and ribosomal protein L39) were down-regulated, suggesting that protein synthesis is not strongly affected by transformation.

Proteases and protease inhibitors
Only the kallikrein B protease and the elafin-like protein II protease inhibitor were up-regulated (3 and 2 fold respectively) after ras^{V12}/E1A-transformation. By contrast, 16 proteases and 7 protease inhibitors were found repressed in transformed MEFs. The tolloid-like (41 fold) and meltrin beta (33 fold) were proteases most down-regulated and the tissue factor pathway inhibitor 2 (44 fold) and the plasminogen activator inhibitor (31 fold) were the most affected protease inhibitors.

Membrane proteins
15 genes encoding membrane proteins were up-regulated and 21 were down-regulated. Histocompability 2, D region locus, (16 fold) and melanoma differentiation associated protein (9 fold) were the most overexpressed genes, whereas Thy-1.2 glycoprotein (36 fold), cadherin 11 (14 fold) and vascular cell adhesion molecule 1 (13 fold) were the most repressed.

Extracellular matrix
Laminin gamma 1 (20 folds) and entactin-2 (6 folds) were the two extracellular matrix encoding genes found up-regulated during transformation, whereas 24 genes were down-regulated. Among them, procollagen type VI, alpha 1 (121 folds), procollagen type III, alpha 1 (56 folds), procollagen type I, alpha 1 (44 folds), procollagen type I, alpha 2 (37 folds), collagen type VI, alpha 3

subunit (21 folds) and decorin (19 folds) were the most affected.

Enzymes

Twelve enzymes involved in cellular metabolism were found overexpressed after ras^{V12}/E1A-transformation and 44 were found down-regulated. The most activated genes were serine hydroxymethyl transferase 1 (6 fold), acetyl coenzyme A dehydrogenase (5 fold) and the acetyltransferase (GNAT) family containing protein (4 fold), whereas the most repressed genes were lysozyme P (88 fold), lysyl oxydase (61 fold) and lysozyme M (55 fold). Interestingly, maximal overexpressions were 6, 5 and 4 fold, whereas down-regulations were 88, 61 and 55 fold indicating that in addition to the fact that more genes were down-regulated (44 vs. 12), change in expression was also more important for down-regulated genes.

DNA-associated proteins

25 genes encoding DNA-associated proteins were up-regulated, whereas no gene of this family was found down-regulated. The most strongly activated genes were nucleoside diphosphate kinase (9 fold), the topoisomerase-inhibitor suppressed (7 fold), the helicase lymphoid specific (6 fold) and the DNA2-like homolog (6 fold).

Cytosolic proteins

Expression of 2 genes encoding cytosolic proteins was activated after ras^{V12}/E1A-transformation, whereas expression of 6 genes was repressed. Genes coding for acyl-CoA-binding protein (3 fold) and tubulin-specific chaperone (2 fold) were overexpressed, whereas the most strongly repressed gene was that coding cytochrome P450 (61 fold).

Channels

5 genes encoding channels were up-regulated and also 5 were down-regulated. Chloride channel protein 3 was the most up-regulated gene (11 fold) and the channel beta-1 subunit (15 fold) was the most down-regulated gene.

Cell growth-associated proteins

As expected for transformed cells which grow more rapidly, 13 genes encoding proteins involved in cell growth were found overexpressed, whereas only 3 were found down-regulated in ras^{V12}/E1A-transformed MEFs. The most activated genes were those coding for cyclin-dependent kinase-like 2 (6 fold) and cell division cycle 7-like 1 (5 fold) whereas the most repressed gene was cyclin D2 (4 fold).

Angiogenesis

Angiogenesis is a key process in carcinogenesis. Contrary to the expected for a tumoral cell, we were unable to found angiogenesis-associated genes up-regulated by ras^{V12}/E1A-transformation. To our surprise, all 8 genes associated with angiogenesis showing differential expression were down-regulated. These included genes coding for thrombospondins 1 (15 fold), 2 (32 fold) and 3 (6 fold), pigment epithelium-derived factor (26 fold), pleiotrophin (24 fold), GRO1 oncogene (16 fold), angiogenin-related protein (4 fold) and tumor necrosis factor induced protein 2 (3 fold).

Apoptosis

8 apoptosis-related genes were up-regulated in transformed MEFs and 3 down-regulated. The p53 apoptosis effector related to Pmp22 was the most activated gene (19 fold) and death-associated protein 1 gene was the most under-expressed (4 fold) after transformation.

Unknown function

3 genes encoding proteins without well defined function were found up-regulated in mutated *ras*-E1A expressing fibroblasts, whereas 8 were found to be down-regulated.

As a proof-of-principle, we verified the relative expression levels of 11 of these 815 genes by Northern blot analysis. The following 11 genes were tested : p8, transgelin, serum amyloid A3, lysyl oxidase, thrombospondin 2, extracellular superoxide dismutase, biglycan, myb, cytokeratin, HMG2 and ezrin. In all of them Northern blot data confirmed microarray data. The first 7 were down-regulated in transformed MEFs, the 4 others being overexpressed (Figure 3).

Discussion

A number of *ras*-regulated genes have been identified by studies on immortalized cells or cancer cells expressing the oncogenic *ras* [14–21]. However, although these results are quite interesting, it is important to note that established cell lines are frequently subject to genetic and epigenetic changes that are selected during passaging or immortalization and may affect *ras* target-gene expression. Primary cultures, such as mouse embryonic fibroblasts, do not have that drawback. This is why, to identify *ras* target genes, we decided to analyze global gene expression shortly after retroviral transfer of an ectopic mutated *ras* in MEFs. Yet, because activated *ras* alone induces MEF senescence instead of transformation, we associated to it the adenovirus-derived oncogene E1A. The ras^{V12}/E1A transformation of MEFs (and of other non-immmortalized cells as well) is specific and controlled. Using the Affymetrix technology on ~12,000 genes, we found that expression of 6.8% of them was significantly modified in MEFs by ras^{V12}/E1A-transformation. Because oncogenic transformation of fibroblasts allows tumor development when cells are injected in the immunocompromised mouse (see Figure 1), studying target genes of activated *ras* should improve our understanding of the molecular mechanisms by which *ras* transforms cells and eventually

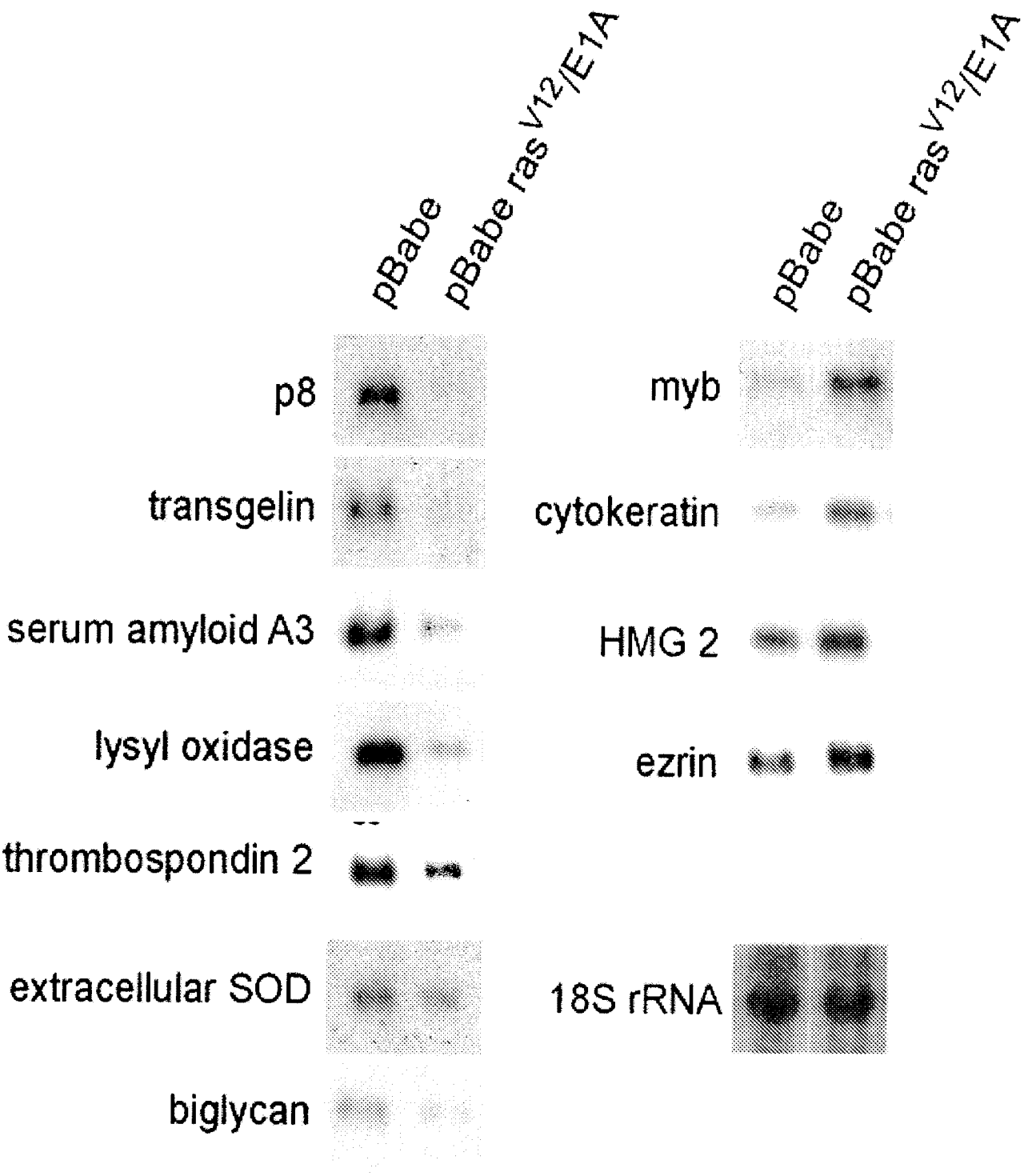

Figure 3
Confirmation of microarray results by Northern blot analysis. 18S rRNA was used as a loading control. Total RNA isolated from pBabe and pBabe-ras^{V12}/E1A transduced MEFs were blotted onto Hybond-N membranes and hybridized with ^{32}P-labeled probes as described in Material and Methods section.

allows tumor formation. It is interesting to note that only 24% of down-regulated and 40% of up-regulated genes showed strong modification (i.e.: >5 fold change) of its expression after transformation.

Several examples of genes up- or down-regulated upon *ras* transformation have already been reported [22–25]. Present data on systematic analysis of about one third of the expressed genome confirm those reports while extending considerably our knowledge of genes activated or repressed by oncogenic *ras* in association with the E1A adenoviral protein. Our results may explain the behavior of transformed cells. For example and as expected, virtually all of the genes coding for secreted factors or extracellular matrix component, which are associated with a differentiated phenotype, were down-regulated. Also, morphological changes observed after transformation (see Figure 1), may be explained by the fact that 44 genes encoding structural proteins were under-expressed. Another expected result was that cell growth-related proteins (involved in the regulation of the cell cycle or inducing cell proliferation) and DNA-associated proteins (involved in DNA replication and reparation) were up-regulated in transformed MEFs, in agreement with their accelerated growth. Also, it is not a surprise to find an altered expression for 56 enzymes involved in cell metabolism because, compared to normal fibroblasts, transformed cells show accelerated growth, increased migration capacity and strong morphological changes. These enzymes could be involved in some of these changes.

Several genes coding for transcription factors (n = 102) and proteins involved in signaling pathways (n = 115) were up- or down-regulated suggesting that modification of the amounts of these factors could be responsible for the dramatic changes in gene expression observed in transformed cells. It is interesting to note that approximately as many transcription factors were up-regulated (n = 57) as down-regulated (n = 45).

Besides data coherent with previous knowledge, we also found very unexpected results. For example, we found that genes coding for proteases and inhibitors of proteases were strongly down-regulated by ras^{V12}/E1A transformation. This was surprising since these factors are up-regulated and strongly involved in tumor progression involving mutated *ras*. This observation could suggest that in human cancers, proteases and protease inhibitors are activated through a mechanism disconnected from *ras* activation. We were similarly surprised by the fact that all 8 angiogenic factors present on the array were found down-regulated by ras^{V12}/E1A transformation. Like proteases and inhibitors of proteases, angiogenic factors are involved in tumour progression and still repressed during ras^{V12}/E1A-mediated transformation. It is therefore highly unlikely that their overexpression reported in several cancers is controlled by a *ras*-dependent pathway. Finally, it was also unexpected that only 5 genes involved in protein synthesis were up- or under-expressed, suggesting that protein synthesis is not strongly altered after ras^{V12}/E1A transformation.

Conclusions

In conclusion, this study of a large number of genes has identified those whose expression is altered upon fibroblast transformation by ras^{V12}/E1A. It is however not exhaustive because the analyzed genes are only representative of the genome (one third of the expressed genes was examined), and post-transcriptional and post-translational modifications were not addressed. Yet, information gathered should be quite useful to future investigations on the molecular mechanisms of oncogenic transformation.

Methods

Primary mouse embryo fibroblasts (MEFs)

Primary embryo fibroblasts were isolated from 14.5 day-old SV129J mouse embryos following standard protocols [26]. Cell were grown in Dulbecco's modified Eagle's medium (DMEM) supplemented with 10% foetal calf serum, 2 mM L-glutamine, 100 IU/ml penicilin G and 100 μg/ml streptomycin.

Retroviral infection

Oncogenic *ras* transforms most immortal rodent cells to a tumorigenic state, whereas transformation of mouse primary cells requires either a cooperating oncogene or the inactivation of a tumour suppressor gene. The adenovirus E1A oncogene cooperates with *ras* to transform primary mouse fibroblasts [7] and abrogates *ras*-induced senescence [27]. Therefore, we transduced MEFs with the pBabe-ras^{V12}/E1A retroviral vector which expresses both the ras^{V12} mutated protein and the E1A oncogene to obtain transformed fibroblasts. pBabe-ras^{V12}/E1A [described in ref. [27]] and pBabe (as control) plasmids were obtained from S. Lowe. Bosc 23 ecotropic packaging (10^6) cells were plated in a 6-well plate, incubated for 24 hr, and then transfected with PEI with 5 μg of retroviral plasmid. After 48 hr, the medium containing the virus was filtered (0.45 μm filter, Millipore) to obtain the first supernatant. MEFs were plated at 2×10^5 cells per 35 mm dish and incubated overnight. For infections, the culture medium was replaced by an appropriate mix of the first supernatant and culture medium (V/V), supplemented with 4 μg/ml polybrene (Sigma), and cells were incubated at 37°C. As a control, we evaluated the ability of the retroviral vector to transduce MEFs by using a retroviral vector expressing the EGFP under control of the retroviral promoter located in the long terminal repeat. About 30% of MEFs expressed high levels of EGFP fluorescence 48 h after

transduction (data not shown), indicating that retroviral vectors are well adapted to our experimental set-up. Retrovirus-infected cells were selected with puromycin (0.7 μg/ml). Transformation of MEFs by the pBabe-ras^{V12}/E1A retroviral vector was evaluated by examining changes in their morphological aspect, by quantifying expression of the RAS protein by western blot, by monitoring cell proliferation, colony formation in soft-agar and tumors in nude mice. In soft-agar assays, pBabe-ras^{V12}/E1A transformed cells formed colonies at high frequency (Figure 1). Similarly, transformed cells produced tumors in all (3/3) athymic nude mice when injected subcutaneously, whereas control MEFs did not (0/3) (Figure 1).

Western blot analysis

One hundred μg of total protein extracted from cells was separated with standard procedures on 12.5% SDS-PAGE using the Mini Protean System (Bio-Rad) and transferred to a nitrocellulose membrane (Sigma). The intracellular level of RAS was estimated by Western blot using the H-ras (C-20) polyclonal antibody (1:200) purchased from Santa Cruz Biotechnology, Inc.

Microarray

Total RNA was isolated by Trizol (Gibco-BRL by Invitrogen). Twenty μg of total RNA was converted to cDNA with SuperScript reverse transcriptase (Gibco-BRL by Invitrogen), using T7-oligo-d(T)$_{24}$ as a primer. Second-strand synthesis was performed using T4 DNA polymerase and E. Coli DNA ligase followed by blunt ending by T4 polynucleotide kinase. cDNA was isolated by phenol-chloroform extraction using phase lock gels (Brinkmann). cDNA was *in vitro* transcribed using the T7 BioArray High Yield RNA Transcript Labeling Kit (Enzo Biochem, New York, N.Y.) to produce biotinylated cRNA. Labelled cRNA was isolated using an RNeasy Mini Kit column (Qiagen). Purified cRNA was fragmented to 200–300 mer cRNA using a fragmentation buffer (100 mM potassium acetate-30 mM magnesium acetate-40 mM Tris-acetate, pH 8.1), for 35 min at 94°C. The quality of total RNA, cDNA synthesis, cRNA amplification and cRNA fragmentation was monitored by micro-capillary electrophoresis (Bioanalizer 2100 by Bioanalyser 2100, Agilent Technologies). The cRNA probes were hybridized to an MGu74Av2 Genechip (Affymetrix, Santa Clara, CA). The MGu74Av2 Genechip represents ~6,000 sequences of mouse Unigene that have been functionally characterized and ~6,000 sequences ESTs clusters. Each sequence in the chip is represented by 32 probes : 16 "perfect match" (PM) probes that are complementary to the mRNA sequence and 16 "mismatch" (MM) probes that only differ by a single nucleotide at the central base (more detailed information about the MGu74Av2 Genechip can be obtained in the web site http://www.affymetrix.com. Fifteen micrograms of fragmented cRNA was hybridized for 16 h at 45°C with constant rotation (60 rpm). Microarrays were processed in an Affymetrix GeneChip Fluidic Station 400. Staining was made with streptavidin-conjugated phycoerythrin (SAPE) followed by amplification with a biotinylated anti-streptavidin antibody and a second round of SAPE, and then scanned using an Agilent GeneArray Scanner (Agilent Technologies). Expression value (signal) is calculated using Affymetrix Genechip software MAS 5.0 (for fully description of the statistical algorithms see http://affymetrix.com/support/technical/whitepapers/sadd_whitepaper.pdf. Briefly, signal is calculated as follow : First, probe cell intensities are processed for global background. Then, MM value is calculated and subtracted to adjust the PM intensity in order to incorporate some measure of non-specific cross-hybridization to mismatch probes. Then, this value is log-transformed to stabilize the variance. Signal is output as the antilog of the resulting value. The 20 probe pairs representing each gene are consolidated into a single expression level. Finally, software scales the average intensity of all genes on each array within a data set. Final value of signal is considered representative of the amount of transcript in solution.

Housekeeping controls β-actin and GAPDH genes serve as endogenous controls and are useful for monitoring the quality of the target. Their respective probe sets are designed to be specific to the 5', middle, or 3' portion of the transcript. The 3'/5' signal ratio from these probe sets is informative about the reverse transcription and *in vitro* transcription steps in the sample preparation. Then, an ideal target in which all transcripts was full-length transcribed would have an identical amount of signal 3' and 5' and the ratio would be equal to 1. Differences greater than three fold between signal at 3' and 5' for these housekeeping genes indicate that RNA was incompletely transcribed or target may be degraded. Ratio of fluorescent intensities for the 5' and 3' ends of these housekeeping genes was <2.

Hybridization experiments were repeated twice using independent cRNA probes synthezised with RNA from two independent sets of MEF-infected cells. Genes were considered as differentially expressed when both hybridizations showed >2 folds change. Data presented in this work represent the average of both hybridizations. The list of unchanged genes should be obtained from authors upon request.

Validation of gene expression profiles by Northern blot hybridization

Synthesis of probes: One microgram of total RNA from MEF cells was subjected to PCR with reverse transcription using the One Step RT-PCR kit (Gibco-BRL) according to the manufacturer's protocol to synthezise specific cDNA probes. PCR were carried out for 32 cycles, each cycle consisting in a denaturing step for 1 min at 94°C, an

annealing step for 2 min at 56°C, and a polymerization step for 2 min at 72°C. Selected RNA species were amplified using the following primers: p8, sense, 5'-ggagagagcagactaggcata-3' and antisense, 5'-gttgctgccacccaagggcat-3'; transgelin, sense, 5'-ccagccagctctgcagatggg-3'and antisense, 5'-gcaggcagatttctgagttc-3'; serum amyloid A3, sense, 5'-ggatgaagccttccattgcc-3' and antisense, 5'-gaagagctacaccgccactc-3'; lysyl oxidase, sense, 5'-taaaacgactgtccccaacc-3' and antisense, 5-tcacggccgttgttagtgta-3'; thrombospondin 2, sense, 5'-aagcccagtcgggcttacgg-3' and antisense, 5-tgctggagctggagccctgc-3'; extracellular superoxide dismutase, sense, 5'-ccttagttaacccagaaatct-3' and antisense 5'-gtacctcaaaggtgctcactgg-3'; biglycan, sense, 5'-ggctgctttctgcttcacagg-3' and antisense 5'-gcaactgaccatcacctccta-3'; myb proto-oncogene, sense, 5'-ctaaaccatttcatgaggag-3' and antisense, 5-aacaaatgcaaaattcaccc-3'; cytokeratin, sense, 5'-ctggtctcagcagattgagg-3' and antisense, 5-ggtaggtggcaatctctgcc-3' ; high mobility group protein 2, sense, 5'-cgtctgccttctgcctgttttg-3' and antisense 5'-gcccttgacacggtatgcagc-3' and ezrin, sense, 5'-caacgaggagaagcggatca-3' and antisense 5'-gtgtgacacctgcctgcagtg-3'. Specificity of the PCR products was confirmed by direct DNA sequencing.

Northern blot hybridization: RNA samples (10 μg) were submitted to electrophoresis on a 1% agarose gel and vacuum blotted onto Hybond-N membranes (Amersham). The filters were hybridized with the ^{32}P-labeled probes for 16 h at 65°C in 5X SSPE (1X SSPE is 180 mM NaCl, 1 mM EDTA, 10 mM NaH_2PO_4, pH 7.5), 5X Denhardt solution, 0.5% SDS and 100 μg/ml single stranded herring sperm DNA. Filters were then washed four times for 5 min at room temperature in 2X SSC, 0.2% SDS, twice for 15 min at 50°C in 0.2X SSC, 0.2% SDS, and once for 30 min in 0.1X SSC at 50°C before autoradiography exposure on Kodak X-Omat films at -80°C from 8 hr to 4 days.

Authors' contributions

SV prepared cells and retroviruses, CM carried out RNA purification and Northern blot analysis, ELC and CL were in charge of microarray hybridization, PB participated in the analysis of gene expression data, JCD participated in the design of the study, JLI participated in the analysis of data and wrote the manuscript. All authors read and approved the final manuscript.

Additional material

Additional File 1

Mouse embryo fibroblasts genes over-expressed upon ras^{V12}/E1A transformation (Microsoft Word document). *Genes found over-expressed by microarray analysis are listed, with their GenBank accession number, the over-expression factors (relative to control) observed in two separate experiments and the average over-expression factor.*
Click here for file
[http://www.biomedcentral.com/content/supplementary/1476-4598-2-19-S1.doc]

Additional File 2

Mouse embryo fibroblasts genes under-expressed upon ras^{V12}/E1A transformation (Microsoft Word document). *Genes found under-expressed by microarray analysis are listed, with their GenBank accession number, the under-expression factors (relative to control) observed in two separate experiments and the average under-expression factor.*
Click here for file
[http://www.biomedcentral.com/content/supplementary/1476-4598-2-19-S2.doc]

Acknowledgements

We thank Dr. S. Lowe for the kind gift of pBabe-ras^{V12}/E1A and pBabe plasmids and R. Grimaud and F. Roche for technical assistance. We also thanks to Dr M.J. Pébusque for critical reading of the manuscript. This work was supported by a grant from the Ligue Nationale Contre le Cancer (LNCC) and Association pour la Recherche sur le Cancer (ARC).

References

1. Capon DJ, Chen EY, Levinson AD, Seeburg PH and Goeddel DV **Complete nucleotide sequences of the T24 human bladder carcinoma oncogene and its normal homologue.** *Nature* 1983, **302**:33-37
2. Shih C and Weinberg RA **Isolation of a transforming sequence from a human bladder carcinoma cell line.** *Cell* 1982, **29**:161-169
3. Barbacid M **ras genes.** *Annu Rev Biochem* 1987, **56**:779-827
4. Newbold RF and Overell RW **Fibroblast immortality is a prerequisite for transformation by EJ c-Ha-ras oncogene.** *Nature* 1983, **304**:648-651
5. H Land, LF Parada and RA Weinberg **Tumorigenic conversion of primary embryo fibroblasts requires at least two cooperating oncogenes.** *Nature* 1983, **304**:596-602
6. Weinberg RA **Oncogenes, antioncogenes, and the molecular bases of multistep carcinogenesis.** *Cancer Res* 1989, **49**:3713-3721
7. Ruley HE **Transforming collaborations between ras and nuclear oncogenes.** *Cancer Cells* 1990, **2**:258-268
8. Hunter T **Cooperation between oncogenes.** *Cell* 1991, **64**:249-270
9. Vogelstein B and Kinzler KW **The multistep nature of cancer.** *Trends Genet* 1993, **9**:138-141
10. Gibbs JB, Oliff A and Kohl NE **Farnesyltransferase inhibitors: Ras research yields a potential cancer therapeutic.** *Cell* 1994, **77**:175-178
11. Langer SJ, Bortner DM, Roussel MF, Sherr CJ and Ostrowski MC **Mitogenic signaling by colony-stimulating factor 1 and ras is suppressed by the ets-2 DNA-binding domain and restored by myc overexpression.** *Mol Cell Biol* 1992, **12**:5355-5362
12. Johnson R, Spiegelman B, Hanahan D and Wisdom R **Cellular transformation and malignancy induced by ras require c-jun.** *Mol Cell Biol* 1996, **16**:4504-4511
13. Finco TS, Westwick JK, Norris JL, Beg AA, Der CJ and Baldwin AS **Oncogenic Ha-Ras-induced signaling activates NF-kappaB**

transcriptional activity, which is required for cellular transformation. *J Biol Chem* 1997, **272:**24113-24116
14. Krzyzosiak WJ, Shindo-Okada N, Teshima H, Nakajima K and Nishimura S **Isolation of genes specifically expressed in flat revertant cells derived from activated ras-transformed NIH 3T3 cells by treatment with azatyrosine.** *Proc Natl Acad Sci USA* 1992, **89:**4879-4883
15. Liang P, Averboukh L, Zhu W and Pardee AB **Ras activation of genes: Mob-1 as a model.** *Proc Natl Acad Sci USA* 1994, **91:**12515-12519
16. Jo H, Zhang H, Zhang R and Liang P **Cloning oncogenic ras-regulated genes by differential display.** *Methods* 1998, **16:**365-372
17. Jo H, Cho YJ, Zhang H and Liang P **Differential display analysis of gene expression altered by ras oncogene.** *Methods Enzymol* 2001, **332:**233-244
18. Shields JM, Der CJ and Powers S **Identification of Ras-regulated genes by representational difference analysis.** *Methods Enzymol* 2001, **332:**221-232
19. Habets GG, Knepper M, Sumortin J, Choi YJ, Sasazuki T, Shirasawa S and Bollag G **cDNA array analyses of K-ras-induced gene transcription.** *Methods Enzymol* 2001, **332:**245-260
20. Brem R, Certa U, Neeb M, Nair AP and Moroni C **Global analysis of differential gene expression after transformation with the v-H-ras oncogene in a murine tumor model.** *Oncogene* 2001, **20:**2854-2858
21. Sers C, Tchernitsa OI, Zuber J, Diatchenko L, Zhumabayeva B, Desai S, Htun S, Hyder K, Wiechen K, Agoulnik A, Scharff KM, Siebert PD and Schafer R **Gene expression profiling in RAS oncogene-transformed cell lines and in solid tumors using subtractive suppression hybridization and cDNA arrays.** *Adv Enzyme Regul* 2002, **42:**63-82
22. Diaz-Guerra M, Haddow S, Bauluz C, Jorcano JL, Cano A, Balmain A and Quintanilla M **Expression of simple epithelial cytokeratins in mouse epidermal keratinocytes harboring Harvey ras gene alterations.** *Cancer Res* 1992, **52:**680-687
23. Hiwasa T, Yokoyama S, Ha JM, Noguchi S and Sakiyama S **c-Ha-ras gene products are potent inhibitors of cathepsins B and L.** *FEBS Lett* 1987, **211:**23-26
24. Contente S, Kenyon K, Rimoldi D and Friedman RM **Expression of gene rrg is associated with reversion of NIH 3T3 transformed by LTR-c-H-ras.** *Science* 1990, **249:**796-798
25. Shields JM, Rogers-Graham K and Der CJ **Loss of transgelin in breast and colon tumors and in RIE-1 cells by Ras deregulation of gene expression through Raf-independent pathways.** *J Biol Chem* 2002, **277:**9790-9799
26. Harvey M, Sands AT, Weiss RS, Hegi ME, Wiseman RW, Pantazis P, Giovanella BC, Tainsky MA, Bradley A and Donehower LA **In vitro growth characteristics of embryo fibroblasts isolated from p53-deficient mice.** *Oncogene* 1993, **8:**2457-2467
27. Serrano M, Lin AW, McCurrach ME, Beach D and Lowe SW **Oncogenic ras provokes premature cell senescence associated with accumulation of p53 and p16INK4a.** *Cell* 1997, **88:**593-602

Pacific Symposium on Biocomputing 6:496-507 (2001)

ON REPORTING FOLD DIFFERENCES

C.L. TSIEN
Massachusetts Institute of Technology and Harvard Medical School
545 Technology Square, NE43-420, Cambridge, MA 02139, USA

T.A. LIBERMANN, X. GU
New England Baptist Bone and Joint Institute, Beth Israel Deaconess Medical Center, and Harvard Medical School, 4 Blackfan Circle, Boston, MA 02115, USA

I.S. KOHANE
Children's Hospital Informatics Program and Harvard Medical School
300 Longwood Avenue, Boston, MA 02115, USA

As we enter an age in which genomics and bioinformatics make possible the discovery of new knowledge about the biological characteristics of an organism, it is critical that we attempt to report newly discovered "significant" phenotypes only when they are actually of significance. With the relative youth of genome-scale gene expression technologies, how to make such distinctions has yet to be better defined. We present a "mask technology" by which to filter out those levels of gene expression that fall within the noise of the experimental techniques being employed. Conversely, our technique can lend validation to significant fold differences in expression level even when the fold value may appear quite small (e.g. 1.3). Given array-organized expression level results from a pair of identical experiments, our ID Mask Tool enables the automated creation of a two-dimensional "region of insignificance" that can then be used with subsequent data analyses. Fundamentally, this should enable researchers to report on findings that are more likely to be in nature truly meaningful. Moreover, this can prevent major investments of time, energy, and biological resources into the pursuit of candidate genes that represent false positives.

1 Introduction

As we enter one of the most exciting times in the history of science, in which genomics and bioinformatics are coming together to make possible the discovery of new knowledge about living organisms at their molecular level, it is imperative that we avoid discovery of "truths" that are not so. While the temptation to plunge into tracing out metabolic pathways, cellular interactions, or genetic regulatory circuits—especially now that we have technologies allowing genome-wide study of RNA expression—is very strong, we must pause long enough to consider how best to report our results such that they may be meaningful. Specifically, for microarray-based expression technologies, whether they are glass microarrays, nylon membranes, or other formats, we need to better understand how to distinguish significant fold difference values from those that fall within the noise level of the experiment at hand.

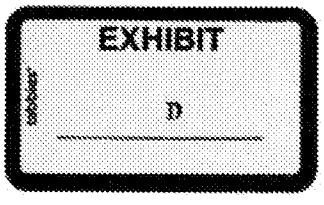

Francis Collins rightfully speculates about the large impact that microarray technology is likely to have, yet reminds us of the "many critically important questions about this new field that are yet unaddressed" [1]. Some have criticized array-based methods for not being model-based, or hypothesis-driven, while others support that the exploratory nature can lead to new hypotheses that then can be tested in the laboratory [2]. Especially because such hypothesis testing of candidate genes, cell-cell interactions, or pathways requires a major investment of time, energy, and biological resources, an important challenge is understanding how to better recognize false-positive results.

We present a "mask technology" by which to filter out those levels of gene expression that fall within the noise of the experimental techniques being employed. Conversely, our technique can lend validation to the significance of fold differences in expression level even when the fold value may appear quite small. Our work is based on the notion that gene expression measurements ought to be repeatable. Fold differences for each corresponding pair of genes in a pair of "identical" experiments should therefore be equal to unity. Identical experiments are ones in which the operating conditions, cell lines, culture media, incubation time, and so forth are controlled to be the same. We first explore whether this is the case by examining several pairs of identical experiments. We then develop the ID Mask Tool, which enables the automated creation of a two-dimensional "region of insignificance" that can be used with subsequent data analyses.

2 Materials and Methods

2.1 Data Collection

The data for this study were collected to evaluate the use of microarray technology for detection of ESE-1 target genes after transient transfection into different cell lines. We hypothesized that a transfection efficiency of greater than 70-80% should be sufficient to detect differences in gene expression between two samples. We first determined the transfection efficiency of various cell lines using a green fluorescent protein (GFP) expression vector. Four of the cell lines tested (HT1080, 293, MCF-7, and MG-63) conformed to the criteria set by us. Total RNA was isolated from MCF-7 human breast cancer cells and MG-63 human osteosarcoma cells transiently transfected with an ESE-1 expression vector 20 and 24 hours after transfection. Experiments were performed in duplicates in order to distinguish, from gene expression, differences due to "biological noise." Specifically, six pairs of these duplicated experiments served as the source of the data that we subsequently used to develop the identity mask methodology. The ESE-1 expression vector also

expressed GFP, which enabled us to confirm transfection efficiencies for each experiment. ^{32}P-labeled cDNA probes reverse-transcribed from these RNAs were hybridized to the Atlas Human cDNA Expression Arrays from Clontech (Clontech Laboratories, Inc., Palo Alto, CA) [3]. Each of these Atlas Arrays (Human 1.2 I, Human Cancer) is a nylon membrane on which approximately 1200 human cDNAs have been immobilized. The hybridization results were analyzed with the software provided by Clontech by normalizing to the signals obtained from housekeeping gene controls on the same array as well as by global normalization. The microarray experiments were validated by RT/PCR using the same RNAs.

2.2 Data Analysis and Mask Creation

We developed the ID Mask Tool, a custom-designed computer program written in the C language, to perform mask creation. The ID Mask Tool takes as input two spreadsheet files corresponding to two identical experiments, along with two user customizable parameters to be discussed below. It returns as output an "identity mask," or ID Mask, specifically for those two experiments.

Each spreadsheet contains the names of several hundred genes and their corresponding brightness intensity levels (as assessed by hybridization of the probe of interest). Only genes present in both files are further considered. For each of these genes, we calculate a "fold difference," the ratio of the intensity in file 2 to the intensity in file 1 for a given gene. All fold values are then sorted based on the corresponding intensity values of the set of genes in the first spreadsheet file. Two parameters are used for creation of each identity mask: intensity range (or sliding window) size, plus either scale value or number of standard deviations. These are used to calculate the ID Mask borders and can be experimented with for better results.

Two methods are then explored for creating identity masks. Method 1 relies on segmental calculation of standard deviations. A "data point" refers to an (x, y) pairing in which x is an intensity value from the first spreadsheet file and y is its corresponding fold difference value (calculated as above). Using all data points in a given sliding window of intensity values (e.g., from intensity level 1001 to 2000), the standard deviation of the fold values is calculated. The average of the intensity values within that window is then paired with a fold value equal to the average fold value within that window plus the number of standard deviations specified by the user. This new pair becomes a candidate "upper mask border" point. Similarly, a candidate "lower mask border" point is created by pairing the average intensity value of that window with the average fold value minus the number of standard deviations specified by the user. Each successive group of data points in each

sliding window of intensity values (e.g., all points from 2001 to 3000, then all points from 3001 to 4000, etc.) likewise gives rise to candidate mask border points.

The set of (*intensity value, fold value*) pairs comprising the candidate upper mask border points is then fit to a line using least-squares linear regression. This line defines the upper mask border. Similarly, linear regression is used to find the lower mask border from the set of calculated candidate lower mask border points. If one of the derived mask borders fits poorly (based upon relationship to original data points), the "reciprocal reflection" of the other mask border can serve in its place. This simply means that each *(x, y)* point on the good-fit (linear) border gives rise to a point *(x, 1/y)* to create the reciprocal reflection border. (See Figures 1 through 6 for examples of mask borders. Figures 2—5 show ID Masks each consisting of one linear regression border and one border derived by taking the reciprocal values of that linear regression border.) The region between these borders represents the "identity" region of insignificant fold differences (i.e., noise).

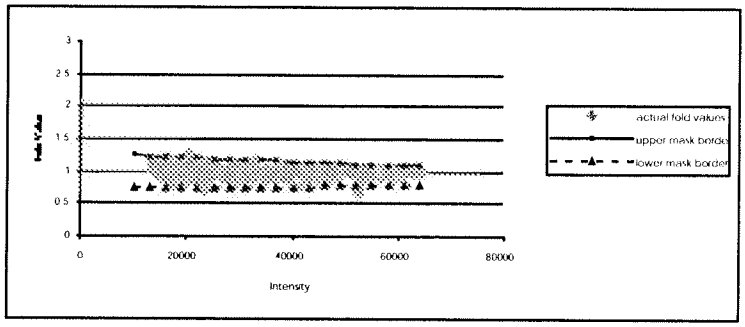

Figure 1: Identity mask for Experiment A. Method 2 with parameters 9000 for intensity sliding window size and 0.975 for scale resulted in the lowest percentage of original data points lying outside of the mask region (0.7%).

Method 2 for creating an identity mask is similar to Method 1 except that candidate mask border points are derived from maximal (and minimal) points in each intensity window rather than from standard deviation calculations. Specifically, amongst all data points in a given window of intensity values, the point with the greatest fold value is chosen. This is repeated for each successive window of intensity values. These fold values can also be scaled before use in linear regression to find the upper mask border. The lower mask border is analogously derived from the smallest fold values.

Once the ID Mask has been derived, all original data points are checked for inclusion or exclusion in the identity mask region. The percentage of data points lying outside of the mask region is reported.

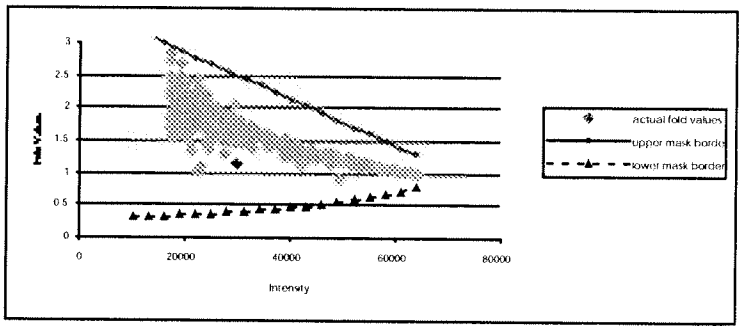

Figure 2: Identity mask for Experiment B. Method 1 with parameters 9000 for intensity window size and standard deviation of 3 resulted in the lowest percentage of original data points lying outside of the mask region (1.7%).

Table 1: Numbers of genes present in each of the experiment pairs, along with the number of genes common to both files in each pair.

	# Genes in 1st File	# Genes in 2nd File	# Genes in Both
Expt A	563	559	550
Expt B	292	516	291
Expt C	244	401	244
Expt D	339	518	326
Expt E	365	397	344
Expt F	233	226	180

3 Results

Six pairs of experiments were performed with Clontech nylon membrane filters and tumor cell lines as described in the Methods section, resulting in twelve spreadsheet files of genes and their corresponding expression intensity values. The ID Mask Tool was used to perform all mask creation experiments as well as basic data analysis. Table 1 displays the number of genes present in each of the file pairs, along with the number of genes common to both files in each pair.

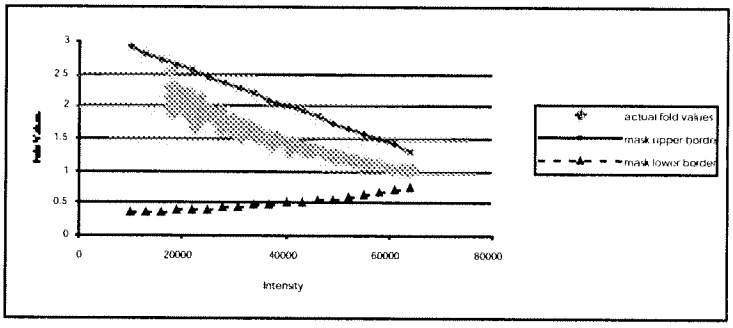

Figure 3: Identity mask for Experiment C. Method 1 with parameters 9000 for intensity window size and standard deviation of 3 resulted in the lowest percentage of original data points lying outside of the mask region (2.0%).

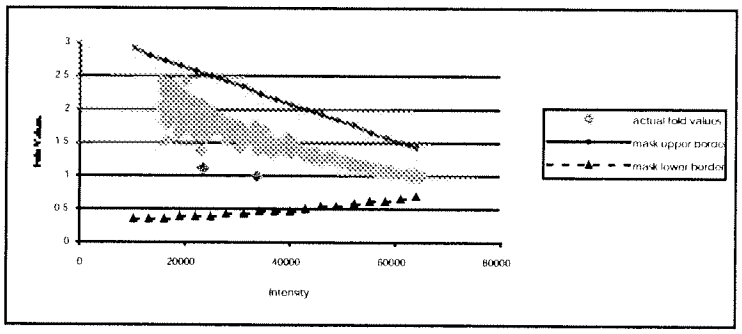

Figure 4: Identity mask for Experiment D. Method 1 with parameters 9000 for intensity window size and standard deviation of 3 resulted in the lowest percentage of original data points lying outside of the mask region (1.5%).

For both Methods 1 and 2 of ID Mask creation, sliding windows of size 1000, 5000, and 9000 on the intensity value axis were chosen for experimentation. Only when calculations were not possible with one of these window sizes (e.g., due to division by zero) was an alternative window size chosen. For Method 1, the number of standard deviations (for calculation of candidate mask border points) was chosen to be 2.5 and 3. For Method 2, the scale factor was chosen to be 0.975 and 1.0.

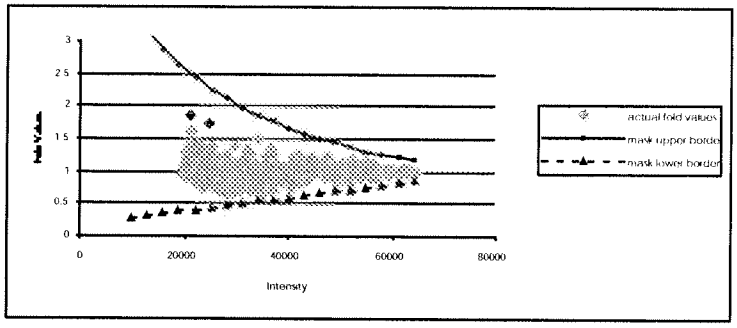

Figure 5: Identity mask for Experiment E. Method 1 with parameters 5000 for intensity window size and standard deviation of 3 resulted in the lowest percentage of original data points lying outside of the mask region (0.9%).

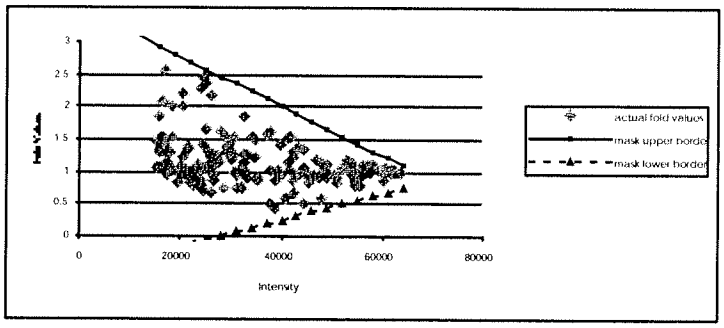

Figure 6: Identity mask for Experiment F. Method 1 with parameters 9000 for intensity window size and standard deviation of 3 resulted in the lowest percentage of original data points lying outside of the mask region (1.7%).

Twelve candidate identity masks were created for each pair of experiments (2 Methods, times 3 intensity window sizes, times 2 scale or standard deviation factors). For each pair of experiments, the ID Mask Tool selected the mask with the lowest percentage of original data points lying outside of the mask region. Figures 1 through 6 show each selected identity mask along with a scatter plot of the original *(intensity value, fold value)* data points for each pair of experiments. Tables 2 and 3 list the percentages of original data points lying outside of the mask region for each of the 12 candidate masks derived for each experiment pair.

Table 2: Each pair of identical experiments gave rise to 12 candidate ID Masks. Six of these twelve were derived by Method 1 (three with standard deviation of 3 and three with standard deviation of 2.5). The other six were derived by Method 2 (three with scale 1.00 and three with scale 0.975). Shown are the percentages of original data points lying outside of the mask region for each of the 12 candidate ID Masks derived for each of Experiments A—C. [σ = standard deviation; intensity range (window) size of 2000 instead of 1000 is used in Experiments B and C for the Method 1 trials.]

	Expt A	**A**	**A**	**Expt B**	**B**	**B**	**Expt C**	**C**	**C**
range size	1000	5000	9000	2000; 1000	5000	9000	2000; 1000	5000	9000
σ = 3	3.1	2.7	2.2	93.2	80.5	1.7	99.6	100.0	2.0
σ = 2 .5	11.1	3.8	3.3	97.3	97.6	2.7	100.0	100.0	2.4
Scale 1.00	19.2	6.2	0.7	100.0	99.0	2.4	100.0	100.0	2.4
Scale 0.975	19.2	6.2	0.7	100.0	99.3	2.4	100.0	100.0	2.9

Table 3: Percentages of original data points lying outside of the mask region for each of the 12 candidate ID Masks derived for Experiments D—F. (See caption in Table 2 for further details.) [σ = standard deviation; intensity range (window) size of 3000 instead of 1000 is used in Experiment D for Method 1 trials, while range (window) size of 2000 instead of 1000 is used in Experiment F for Method 1 trials.]

	Expt D	**D**	**D**	**Expt E**	**E**	**E**	**Expt F**	**F**	**F**
range size	3000; 1000	5000	9000	1000	5000	9000	2000; 1000	5000	9000
σ = 3	17.1	88.4	1.5	0.9	0.9	0.9	5.5	6.1	1.7
σ = 2 .5	24.5	99.4	1.5	2.6	2.0	2.9	7.2	6.6	2.8
Scale 1.00	100.0	99.7	2.4	43.8	18.6	19.7	53.0	9.9	10.5
Scale 0.975	100.0	99.7	3.4	44.3	20.0	20.0	54.7	9.9	11.6

4 Discussion

DNA microarrays clearly are making a large impact on the way we approach problems in molecular biology and genomics. These devices are enabling the genome-wide study of expression in *Escherichia coli* K-12, for example [4]. Others are using DNA microarrays in the study of B-cell lymphomas [5], growth control genes [6], and aging [7]. Some researchers are focusing on developing new [8] or using existing [9] clustering techniques to facilitate the analysis of all the data made available by this relatively new technology. Few, however, have focused specifically on studying the properties of these array data to better understand how to distinguish significant from insignificant "findings."

One way we might be able to better discern meaningful discoveries from the rest is by applying an identity mask technology, such as the one we have presented. Our experiments show that greater amounts of biological noise are present at lower gene expression levels. Thus, there is no magical absolute cut-off for a meaningful fold value. There does appear to exist, however, a "mask of insignificant values," outside of which the fold values are more likely to represent true significance. In Figure 6, for example, a fold difference of 1.5 may be meaningful at an intensity level of 60,000, while a fold difference of 2.5 may be insignificant at an intensity level of 20,000. This result is in stark contrast to a study by Incyte Pharmaceuticals [11], in which they conclude: "any elements with observed ratios greater than or equal to 1.8 should be deemed differentially expressed." A brief glance at the microarray-related literature will quickly confirm that others are also reporting particular fold difference values, such as 1.8, as significant [7]. We argue, however, that the significance of a fold change depends upon the intensity value; genes that are expressed at low levels and hence have weak intensity signals need to show a much greater fold difference than highly expressed genes.

Some have proposed simple statistical tests to determine whether fold differences are significant; t-tests, for example, are included in the GeneSpring software package (Silicon Genetics, San Carlos, CA). Lee *et al.* propose a statistical method using normal distributions and posterior probabilities to determine the likelihood that a gene is truly expressed in a tissue sample [12]. Methods like these are no doubt important; used alone, however, they may under-emphasize the correlation between fold values and intensity values. Future efforts might explore how to best use statistical validation techniques in conjunction with the identity mask method.

While our study used Clontech filters, the general techniques presented for understanding identity masks of insignificance apply to all different types of expression arrays. Both nylon membrane and glass slide array techniques have their

individual advantages. Nylon membrane arrays have sensitive detection using hybridized ^{32}P probes. Glass microarrays have high-resolution fluorescent detection, dual labeling for hybridizing two probes on a single array, and ease in automated handling of slides [3]. Richmond *et al.* compared hybridization of radioactive cDNAs to spot blots on nylon membranes with fluorescence-based hybridization to glass microarrays; they found both methods to be reliable and reproducible [4]. Chen describes a colorimetry detection system for use with nylon membranes [13].

Regardless of the specific array format employed, it seems clear that a custom-derived identity mask is one method that could help improve appropriate reporting of fold difference results. Future work should include an exploration of fitting curves rather than lines for the mask borders. The upper mask border in Figure 2, for example, may benefit from a fitted curve, or at least a piecewise linear model.

An alternative method for mask creation might be to always calculate fold differences greater than 1 by simply swapping the order of individual intensity values whenever the fold value is less than 1. Only the upper mask border would then need to be created. (The lower mask border would be the unity fold difference line.)

It is not clear why there were some large differences between the numbers of genes detected in the experiment pairs of Experiments B, C, and D. These may have been due to experimental error or biological noise. Interestingly, the identity masks for these three also do not fit as nicely as those for Experiments A, E, and F.

While we have selected from amongst the candidate identity masks those with the lowest percentages of points outside the mask region, future work might consider refining the mask fit to purposely exclude approximately 5% of the data points. This could be likened to $p < 0.05$, in which 5% of the time, we may inadvertently report a result as significant even though it is not. A potential benefit is a closer overall mask fit and therefore less likelihood to call a significant finding insignificant.

In only one out of the six pairs of experiments did Method 2 (scaling values) perform better than Method 1 (standard deviations). This is possibly due to the mathematical basis upon which standard deviations are calculated, making them in general more robust and accurate. One way in which scaling actual data points can fail is when there exist outliers. Another is with the choice of too small an intensity window size. This can lead to a sort of "overfitting" problem; our group of candidate "maximum" points from which to derive the upper mask border may then contain several non-maximum values. In Tables 2 and 3, there is a definite trend of worsening mask fit as one decreases the intensity range (window) size from 9000 to 1000. It is likely that in most applications, Method 1 may be more suitable.

Our aim has been to provide a foundation for evaluating fold values. The ultimate goal is to find truly significant fold differences when performing "treatment versus control" comparisons. Analyses of those types of comparisons will likely further our understanding of the masking technique as well. Especially because we recognize the use of DNA microarrays as a method by which to explore the genome in a model-independent fashion [10], it is imperative that we have a basis for judging exploratory findings as being important or simply "in the noise." Candidate genes found through exploration can lead to investment of significant resources; we need to avoid such pursuits of false positive findings.

Acknowledgments

The authors would like to thank Atul Butte, M.D. for assistance with references, and the members of Towia Libermann's laboratory for performing the hybridization experiments.

References

1. F.S. Collins, "Microarrays and macroconsequences" *Nature Genetics* Suppl. **21**, 2 (1999)
2. "The chip challenge" *Nature Genetics* **21**, 61-62 (1999)
3. Clontech web page at http://www.clontech.com/about/index.html
4. C.S. Richmond, J.D. Glasner, R. Mau, et al., "Genome-wide expression profiling in Echerichia coli K-12" *Nucleic Acids Research* **27**, 3821-3835 (1999)
5. A.A. Alizadeh, M.B. Eisen, R.E. Davis, et al., "Distinct types of diffuse large B-cell lymphoma identified by gene expression profiling" *Nature* **403**, 503-511 (2000)
6. F. Bertucci, S.V. Hulst, K. Bernard, et al., "Expression scanning of an array of growth control genes in human tumor cell lines" *Oncogene* **18**, 3905-3912 (1999)
7. C.-K. Lee, R.G. Klopp, R. Weindruch, et al., "Gene expression profile of aging and its retardation by caloric restriction" *Science* **285**, 1390-1393 (1999)
8. M.B. Eisen, P.T. Spellman, P.O. Brown, et al., "Cluster analysis and display of genome-wide expression patterns" *Proc. Natl. Acad. Sci. USA* **95**, 14863-14868 (1998)
9. A.J. Butte and I.S. Kohane, "Mutual information relevance networks: functional genomic clustering using pairwise entropy measurements" *Proceedings of the Pacific Symposium on Biocomputing* (2000)

10. P.O. Brown and D. Botstein, "Exploring the new world of the genome with DNA microarrays" *Nature Genetics* Suppl. **21**, 33-37 (1999)
11. "GEM microarray reproducibility study" Incyte Technical Survey, Incyte Pharmaceuticals, Inc. (1999)
12. M.T. Lee, F.C. Kuo, G.A. Whitmore, et al., "Importance of replication in microarray gene expression studies: statistical methods and evidence from repetitive cDNA hybridizations" *PNAS* **97**, 9834-9839 (2000)
13. J.J. Chen, R. Wu, P.C. Yang, et al., "Profiling expression patterns and isolating differentially expressed genes by cDNA microarray system with colorimetry detection" *Genomics* **51**, 313-324 (1998)